Visuomotor integration and visuomotor skill learning depend on local plasticity in visual cortex during development

Inauguraldissertation

zur

Erlangung der Würde eines Doktors der Philosophie

vorgelegt der

Philosophisch-Naturwissenschaftlichen Fakultät

der Universität Basel

von

Felix Widmer

Basel, Switzerland, 2023

Genehmigt von der Philosophisch-Naturwissenschaftlichen

Fakultät auf Antrag von

PD Dr. Georg Keller (Erstbetreuer)

Prof. Dr. Andreas Lüthi (Zweitbetreuer)

Prof. Dr. Mahesh Karnani (externer Experte)

Basel, den 25.05.2021

Prof. Dr. Andreas Lüthi Prof. Dr. Marcel Mayor

TABLE OF CONTENTS

ACKNOWLEDGEMENTS

I would like to thank Georg, who guided my research during my PhD and gave me the opportunity to study and do research at the Friedrich-Miescher Institute (FMI) in Basel, which is especially meaningful because I arrived as an undergraduate and medical student with no formal training or background in neuroscience or science in general. His advice, of personal and professional nature, was instrumental to proceed to this point.

Thank you to my thesis committee members, Tania Barkat, Dragos Inta, Mahesh Karnani, Andreas Lüthi and Botond Roska for helpful scientific advice, their advice helped guide and shape this work.

To all Keller group and Keller alumni: Thank you for the fun, and the help I received (coding, technical and scientific), and for all the previous work, including millions of lines of code that were readily available for me and took years to develop, and made my work possible. Thank you to Alex and Bo for providing the basis for my project. Thank you also to our technicians, Tingjia and Daniela, who produced all of our viruses, helped to design new constructs, helped with the mouse line maintenance and genotyping and navigating the lab environment. A thankful note to Matthias, who provided feedback on scientific writing when I was applying to the group. Thank you to the FMI and facilities. To all of the FMI IT, especially Dean Flanders, thank you for the support, openness, flexibility, transparency and for being highly effective and reachable, at all times. To Paul and Peter in the workshop: thank you for your help, and for friendly and rich discussions. Thank you to Anna, Baba, Becky, Bo, Matthias, Lukas, Sean and Tingjia for taking an unreasonable amount of time to provide helpful comments on earlier versions of this manuscript, which I truly appreciate.

My friends from medical studies and before I thank for emotional support and shedding light on life outside research, like a two-week bike-ride in Norway (Rallarvegen). My musical friends at FMI and the university orchestra I thank for wonderful rehearsals and concerts, entertaining evenings, advice, and discussions.

Last but not least, I would like to thank my very supportive parents and family, and my partner, Patricia Repáraz, without whom this work would not have been possible.

Thank you.

ABSTRACT

Visuomotor experience shapes responses in visual cortex during development. Coupling between movement and visual feedback establishes a comparator circuit between top-down and bottom-up inputs in layer 2/3 of mouse primary visual cortex (V1). Such a circuit is capable of computing prediction error responses in layer 2/3 excitatory neurons in V1. Given that visual cortex receives both the bottom-up visual input and signals consistent with a top-down prediction of visual flow given movement, it has been speculated that visual cortex is a site of integration of these two signals. If correct, we would predict that perturbing plasticity in V1 during development should prevent the establishment of a normal balance between bottom-up and top-down input, and consequently an impairment of visuomotor prediction errors in layer 2/3 neurons of primary visual cortex .

In **Chapter I**, we tested whether local plasticity in visual cortex is necessary for the establishment of this balance by locally perturbing neural plasticity. Our results show that perturbing NMDA receptor-dependent plasticity during development of the visual system leads to a reduction in visuomotor prediction error responses, and that plasticity in V1 is crucial for the development of normal visuomotor integration.

In **Chapter II**, we further investigated the balance of top-down and bottom-up inputs in V1 and ask, given that pro-psychotic agents (e.g., hallucinogens) can influence visual cortex activity, whether antipsychotic drugs also induce common circuit changes. We investigated three antipsychotic drugs: Haloperidol, Clozapine and Aripiprazole, with the aim of identifying a common functional signature, possibly underpinning their clinical efficacy. The most common change was a decrease in visuomotor prediction errors in layer 2/3 neurons. Clozapine, as one of most effective drugs, decreased activity of inhibitory neurons thought to mediate visual feedforward signals and increased the mean activity in layer 5. Overall, however, we did not find common changes in all of these three antipsychotic drugs.

INTRODUCTION

PROLOGUE Note: this section is intended as an illustrative introduction to predictive processing

To them, I said, the truth would be literally nothing but the shadows of the images. ~ *Plato, The Republic, Book VII(Plato)*

In Plato's allegory of the cave, prisoners chained since birth only ever see shadows of objects cast on a wall. With nothing else to do, the prisoners invented a game to guess the guards based on the shadows cast. The prison guards, having come to know about this, would indulge in a rather depraved game of their own, where they would fool the prisoners by moving puppets across the fire to cast human-like shadows (a notion recapitulated in Descartes' evil demon, or the simulation theory). What if, not unlike the prisoners in this allegory, we are limited in our access to reality – not through chains, but through the limitations of what we can see or hear, 'shadows' of what our senses report? And, if what we see is influenced by the experience throughout life, how accurately do they mirror reality?

Our perception (lat. *perception*; gathering, receiving) is the interpretation of the sensory information reported by our sensory organs, like our eyes (more specifically, the retina). To perceive, we constantly filter relevant from redundant signals. And our perception mastered this task, constantly making predictions, that are based on our knowledge and experience that one has accumulated over one's lifetime. As an example, have a look at **Figures 1A (left).** On first glance, the image may seem like nothing but meaningless TV-static (noise), however once we are told there is a Dalmatian hidden in the image (**Figure 1A, right**), it instantly becomes interpretable.

A

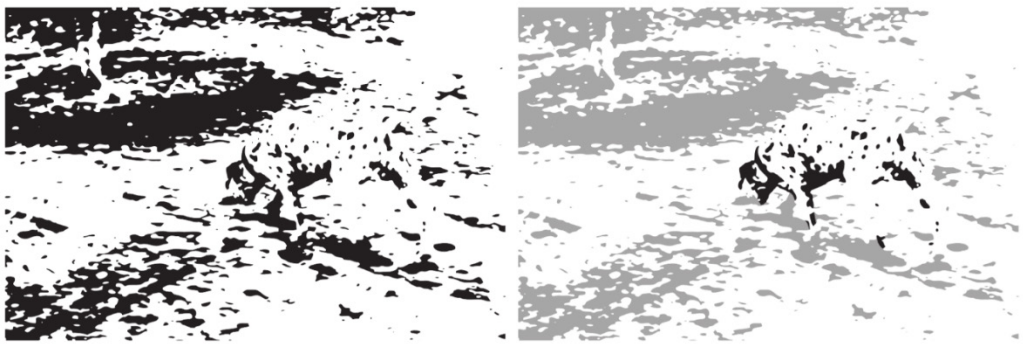

Figure 1A. Emergent image of a dalmatian, by R.C. James.

B

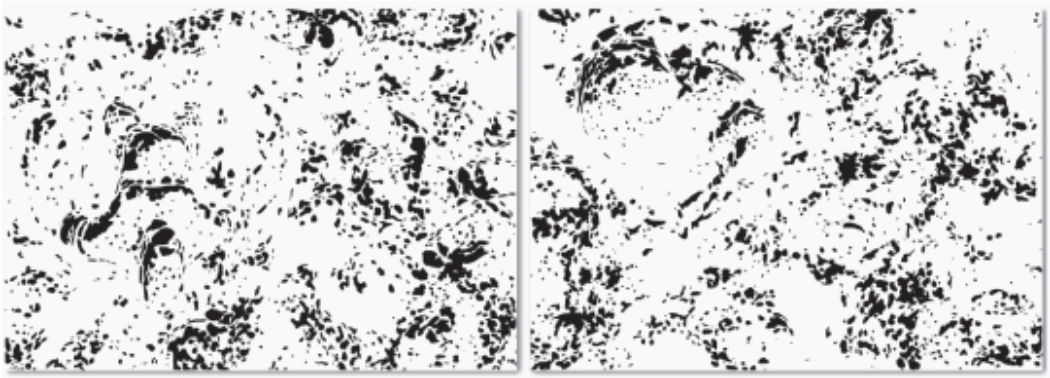

Figure 1B: In the emergent images presented above, noise becomes interpretable when the objects orientation corresponds to 'the expected pose': Flip the image upside down to facilitate the perception of two animals (one left, one right). Once the gorilla and rabbit are identified, they can easily be perceived without the upside-down flip (Mitra et al., 2009)

In fact, once knowledge has been obtained about what objects are displayed in this noisy image (**Figure 1A, right**), the object often becomes immediately recognizable, and the prediction is so strong that it is almost impossible to ignore this percept ('unsee', **Figure 1A, left**). Similar examples exist in other sensory domains. In the auditory domain, artificially distorted speech (e.g, sine-wave speech) seems unintelligible until the clear, undistorted version is presented (reminiscent of 'secret messages' found in popular music when played in reverse). In the somatosensory domain, we can assume feeling touch and even a sense of ownership of a rubber hand (rubber hand illusion). A similar 'trick' is exploited in the clinical setting (mirror therapy) to lessen the reported pain of patients in limbs that have been previously amputated or do not exist anymore for other reasons (phantom pain).

C_n y_u st_ll re_d t_is?

Our predictions are continuously filling-in 'missing' sensory information. In vision, a prime example is the constant obscuration of our visual field by what is known as the 'blind spot', a place on the light-detecting organ (retina) that lacks light detecting rods and cones because of perforating nerve fibers exiting the eye– yet we perceive a congruent visual scene despite this lack of information.

Predictions of sensory information goes beyond basic pattern completion, one combines information across sensory modalities to make predictions. Many people navigate to their bathroom at night, even in complete darkness (the brain receives no visual information), where the experience is described as navigating through an internal visual map, that can be vividly imagined with information acquired through other senses (e.g., touch, hearing). We are also able to predict likely outcomes of complex motor actions, such as whether we are able to catch a ball or not during sports. When presented with a natural scene, we may predict 'what's next' based on remarkably intricate concepts like 'water flows downward' and 'probably someone is playing a prank' (**Figure 2**).

Figure 2. *What's next?* We generate remarkably complex predictions with ease. It is clear, that the person on the left will 'take a shower' soon after this picture is taken. Besides the immediate and unconscious separation of foreground and background in this picture, we form predictions that require detailed knowledge of remarkably complex and abstract concepts like the behavior of flowing water and how it interacts with gravitational forces, and social constructs of what makes a prank and about the likely emotional state of both persons. Credit: Dr. Keller (left), Dr. Heindorf (right).

Further, it is worth pointing out how difficult these problems are, by looking at how hard it is to implement them in robotics and computer science. Computers may accurately display images in different shades and colors, but it is much harder to separate 'foreground' from 'background' in a natural scene; or selectively focus on a particular conversation in a room filled with people (cocktail party problem). In movies and pictures (e.g., **Figure 2**) we can easily predict 'what's next', a highly sought-after feature for data compression, but computers struggle.

Based on previous experience, our predictions about sensory information enhance and guide our interpretation. In this manner, however, predictions add a distortion to our perception of the external world. This distortion is obvious when those predictions interfere with sensory information *per se*, e.g., in a sensory illusion. In optical illusions, for example, we can easily prove (**Figure 3**) that our predictions about objects retaining their color independent of illumination (e.g., time of day) deviate from reality (color constancy). Predictions may even override visual perception (colloquially described as 'we see what we want to see'): In a text we have seen many times and check for errors, we read over the most obvious mistakes, and given a task of predicting how many passes have been given between a basketball team, we miss a gorilla walking by in the same video (Simons and Chabris, 1999).

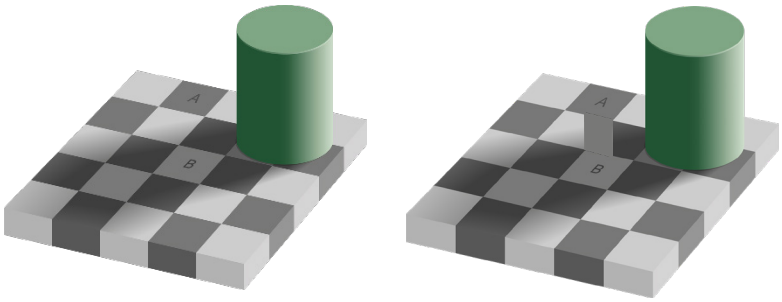

Figure 3. Checkerboard illusion by Edward H. Adelson. Left: Our predictions of color constancy make tile 'B' seem brighter than 'A'. Right: Connecting the tiles makes the optical illusion apparent: Both tile 'A' and 'B' are the same shade of grey.

What could be the evolutionary advantage of having this predictive ability, that distorts our perception of the external world, beyond direct representation of the light entering our eyes? One current prevailing theories of brain function (*predictive processing*) suggests animals actively construct a *generative internal model* of the world, based on previous experience and the behavioral relevance of stimuli. This internal and dynamic representation of the statistics of the outside world, would allow us to quickly separate foreground and background from an image. This may help us identify the threat and distance of a predator, while predicting 'what's next' may help us to run from a threat or pre-emptively avoid it.

In this way, internal models may be used to form predictions of sensory consequences, indicating a causal relationship from A (touch a hot stove) to B (feeling of pain and heat). The constructed and generative nature of internal models, however, is illustrated when this model is used inversely (I feel heat and pain; am I touching a hot stove?). This may explain the observations obtained from split-brain patients, where as a measure of last therapeutic resort in patients suffering from treatment resistant epilepsy, their two sides of the brain (hemispheres) are physically separated (by surgically severing the corpus callosum). When one hemisphere is asked to perform a task (e.g., 'open the window') and the other hemisphere, observing the action (and without knowledge of the task) is asked to explain *why* the task was performed – it comes up with a make-believe explanation, a typical answer would be 'I felt it was a bit warm and stuffy in the room, so I opened the window'.

"What I cannot create, I do not understand." —Richard Feynman

In this case, the internal model does not inform of probable sensory consequences (A -> B), instead inversely, the sensory consequences inform of probable sensory information (B -> A, colloquially known as a 'best guess of what's happening'). This is also illustrated in another experiment where 50% of participants were able to provide (or rather, generate) descriptions, given a fake childhood picture, even though that event never took place (Wade et al., 2002); or may explain observations in the Charles Bonnet syndrome, where patients lose their vision (but not other senses) yet still seem to perceive (or rather, hallucinate) visual scenes (Reichert et al., 2013). This generative aspect of internal models can explain how we can imagine probable futures, how we may navigate a dark room according to an imagined visual representation of the environment.

As a sidenote, the computational advantage of generating sensory input data (A), based on a prediction (B) is made clear when this idea is translated into the field of machine learning (e.g., generative adversarial networks, GANs). Here, based on example images, a 'generator network' comes up with new, imaginary input (A, e.g., a variety of birds) and helps to train a second, classifier network that forms predictions based on that data (B, e.g., 'is this a bird or not?'). Compared to previous methods which focused solely on the latter, the predictive network structure (A -> B), adding this generative component (B -> A) enables the network to seemingly grasp abstract concepts thought to require human knowledge; these networks can re-paint drawings and photographs in 'Monet-style' (Style-GAN (Brown et al., 2020)), write realistic news articles given only one single start sentence (GPT-3 (Brown et al., 2020)), or transform a personal home video recording into a realistic presidential speech spoken by a president (deep fake). Therefore, at least in the field of machine learning, the addition of generative networks added new functionalities and advantages.

Given this framework, and the fact that multiple people disagree about predictions based on sensory input from something as simple as the colors of a dress (**Figure 4A**) and that we can even switch our perception of identical visual information at will (**Figure 4B**), contemporary philosophers like Andy Clark (Clark, 2013, 2016) discuss how much of our perception is guided by internal models ('controlled hallucination'), rather than direct sensory information. How sensory information and predictions might be balanced and how this balance is initially established, tuned and shifted, is a matter of current debate and research (including some the work presented in **Chapter I and II**).

A

B

Figure 4. A: Colored dress illusion. Depending on the lighting condition, the colors of this dress are either perceived black and blue, or gold and white designed by (Roman Originals), published Feb. 2015). **B**: Young or old woman? What you see depends not only on your own age and experience (Nicholls et al., 2018) but the perception can be switched back and forth at will (more colloquially: 'we see what we want to see').

Learning of internal models is thought to occur through minimizing prediction errors, which may lead to updated and refined models in both directions (recapitulate progressively more realistic sensory data and derive more accurate predictions from it). Effectively minimizing prediction errors and building more accurate internal models are a highly desirable trait in human society: In sports, a good internal model of which sets of muscle contractions lead to consistently hitting a ball with a stick and into a hole in the ground, kilometers away, is recognized as extraordinary and is monetarily rewarded. On the opposite spectrum, internal models that poorly capture these relationships, or are temporarily perturbed, are considered abnormal (hallucinogenic drugs) or pathological (psychiatric disorder). Understanding how this balance is shifted may help understand how similar clinical symptoms may converge in psychiatric disorders, an idea we explored in **Chapter II**.

Much previous research in the field of vision and visual perception has gone into the characterization of basic/high contrast stimulus responses, such as vertical and horizontal, white and black bars. Previously, it was thought that visual information would be progressively filtered (and combined with other sensory information), the further it propagates away from the sensory organ. After an invariant representation is formed, another brain area would decide how to act on that information. It is clear from these enormous efforts, that the primary visual cortex robustly responds to a variety of different visual stimuli. What is much less clear, however, is how distortions of perception, and balance of visual input and predictions, are integrated.

A recent review summarizes experimental evidence consistent with the idea of an internal model that gives rise to predictions of sensory information and consequences, that likely have a profound influence on visual perception (Keller and Mrsic-Flogel, 2018). One line of evidence consistent with the idea of internal models comes from the discovery of sensorimotor prediction error signals in primary visual cortex of mice (Keller et al., 2012). This response (generated by a group of layer 2/3 excitatory neurons) occurs when there is a violation of prediction. To show this experimentally, mice played a video game, where they ran through a virtual tunnel. The speed a mouse advanced through the tunnel (visual flow of the tunnel) is a result of their movement, and directly under the mouse's control and up to its motivation to run (closed-loop). At random times, this coupled experience is suddenly perturbed with a transient halt of visual flow – the equivalent of a video game freezing, statically displaying the last frame for some time. This event (visuomotor mismatch) results in a large neuronal response that reports a signal consistent with the idea of a mismatch between predictions of visual flow (based on the animals' movement) and the resulting visual flow. Subsequent research showed that these specific prediction error responses are not innate, and develop with experience (Attinger et al., 2017). Characterizing circuit elements consistent with this idea is at the heart of the research I have come to learn about and contribute to with my work. In humans, internal models can be probed by verbal inquiry (e.g., 'why do you think touching a hot stove will lead to a feeling of heat and pain?'). However, beyond the realm of verbal communication, we have far few tools (if any) to directly probe internal models. In other animals, like mice, we have established sophisticated tools for visualizing and manipulating live brain activity. Unsurprisingly however, accessing internal models in mice is a lot harder, requiring more sophisticated experimental paradigms. Nevertheless, it is possible to at least build and manipulate the sensory experience of the animal and violate what we can assume would be strong predictions of the internal model, as is the case for the aforementioned visuomotor mismatch. Furthermore, we can examine which drugs and molecular mechanisms shape these (putative) prediction error responses. This will be elaborated on in **Chapter I and II**.

VISUAL SYSTEM OF THE MOUSE

In this chapter, I would like to briefly review and introduce the visual system of the mouse. It has become an essential model system for research because of the vast toolkit that enables a researcher to turn off and on brain cells (neurons) using light (optogenetics), genetically target specific neuronal subpopulations for recording and manipulation, and turn off and on genes at defined timepoints. Genetics, relatively short breeding times and low cost compared to other mammals have also made mice a workhorse in the systems neuroscience field. Despite the differences between the human and mouse visual system (e.g., mice do not have a fovea), the mouse visual system is a useful model to interrogate cortical processing of vision. The arguments as to why are summarized elsewhere and are outside of the scope of this thesis (Huberman and Niell, 2011).

For a brief review of the visual pathway: photoreceptors in the retina convert light into electrical signals, which are transmitted and filtered and forwarded by local neurons. Signals are passed on to the output neurons of the eye, the retinal ganglion cells (RGCs), of which there are many subtypes (e.g., direction-selective). RGCs then project to many subcortical brain areas (Morin and Studholme, 2014) with different functions. Relevant to cortical processing of sensory information is the thalamus, more specifically the dorsal lateral geniculate nucleus (dLGN). This area is thought to relay signals from multiple different kinds of RGCs to the neocortex. dLGN outputs directly to cortex in a topographic manner (retinotopic), typically (but not always) from the contralateral retina (Rompani et al., 2017). Different regions of dLGN further process (Erisken et al., 2014) and send their inputs to other areas and primary visual cortex (V1). Cortex can be divided into morphologically distinct laminae. In the mouse, these are typically separated into layers 1, 2/3, 4, 5 and 6. The core region of dLGN projects mainly to layer 4 (but also layer 5 and 6), other parts (e.g., the shell region) project mainly to layer 1 (Cruz-Martín et al., 2014; Hooks and Chen, 2020). dLGN also receives retinotopically aligned feedback (as opposed to feedforward, from the retina) projections from V1 from layer 6 (Bickford et al., 2010; Seabrook et al., 2017). The reciprocal connection between thalamus and cortex is sometimes also referred to as corticothalamic loop (Guo et al., 2017). Although there are numerous details and exceptions we can largely think of the visual system as consisting of a stream of information emanating from the retina, passing through a portion of the thalamus and reciprocally connected to the visual portion of cortex, where the information is further processed and propagated to other parts of the brain.

V1 anatomy. V1 receives feedforward input from the retina via LGN and receives strong feedback input from reciprocally connected, neighboring visual areas. V1 also receives feedback input from a diverse set of cortical areas (mainly targeting layer 1), like auditory or motor-related areas that target specific groups of neurons within those layers (Callaway, 2002; Ibrahim et al., 2016; Leinweber et al., 2017). Neurons in V1 (and the rest of neocortex) can be very coarsely divided into excitatory (pyramidal) neurons and numerous, differing inhibitory neuronal subpopulations with the major groups being represented by those of which are somatostatin-expressing (SST), parvalbumin-expressing (PV) and vasoactive intestinal peptide-expressing (VIP) neurons. These subpopulations, and many more, can be specifically targeted using transgenic mouse lines and have distinct roles within the neocortical circuit.

V1 function. Neurons in V1 that respond to high contrast alternating black and white bars were first reported in cat and monkey visual cortex (Hubel and Wiesel, 1962). The term 'receptive field' was coined in 1906 by neurophysiologist Charles Sherrington in the somatosensory context (Sherrington, 1906), and was adapted to visual system by Hartline (Hartline, 1938), referring to a region in visual space which optimally activates a neuron in V1. Previously, there was debate about how much of V1 responds to visual stimuli (Masland and Martin, 2007; Olshausen and Field, 2009). Recently, one study generated a systematic and large (nearly 60'000 neurons), publicly available dataset of V1 responses to visual stimuli, stratified by different neuronal subpopulations and cortical layers, addressing this debate. The study estimates a large part (77%) of V1 neurons respond to at least one of the presented stimuli, many showing classical tuning properties, such as orientation- and direction-selective responses to gratings (de Vries et al., 2020). Based on multiple such findings, the representational framework suggests that visual cortex functions to form a representation of external stimuli, and this representation becomes increasingly complex at higher hierarchical levels (Marr, 1982). Lower levels would classify bars and edges, and higher levels would integrate these signals to form more complex features like 3D objects.

Besides responding to classical visual stimuli, neurons in V1 can also differentiate complex visual stimuli from the surround and can modulate their responses depending on behavioral context, such as locomotion, and it is thought that feedback connections contribute to this computation (Keller et al., 2020; Niell and Stryker, 2010; Schnabel et al., 2018). It is unclear however why feedback projections from other areas (such as auditory cortex, similarly organized tonotopically) map onto feedforward inputs within V1 and modulate activity (Ibrahim et al., 2016) and how activity in the absence of retinal input can be explained (Keller et al., 2012). Predictive processing provides a unifying framework that provides explanations about the nature and purpose of these feedback connections.

PREDICTIVE PROCESSING AND THE REPRESENTATIONAL FRAMEWORK.

How do biological systems distinguish between self-generated and external sensory events? When we turn our head to the left, we generate visual flow to the right on the retina. On a perceptual level, however, the world remains static. Predictive processing suggests that one way to disentangle external sensory input (world is moving) versus self-generated input (head movement) is to use a copy of the motor command to predict the self-generated input and subtract the sensory input – the remainder is external.

Specifically, predictive coding suggests that the brain is equipped with an internal model of the world. The internal model captures statistics of previous experience and encodes predictions as parameters of a generative model. Similar ideas have been formalized by different brain research fields (Franklin and Wolpert, 2011; Friston, 2005; Rao and Ballard, 1999; Spratling, 2017). Following Andy Clark (Clark, 2016), a recent review (Keller and Mrsic-Flogel, 2018) refers to this family of theories as the predictive processing framework (**Figure 5**).

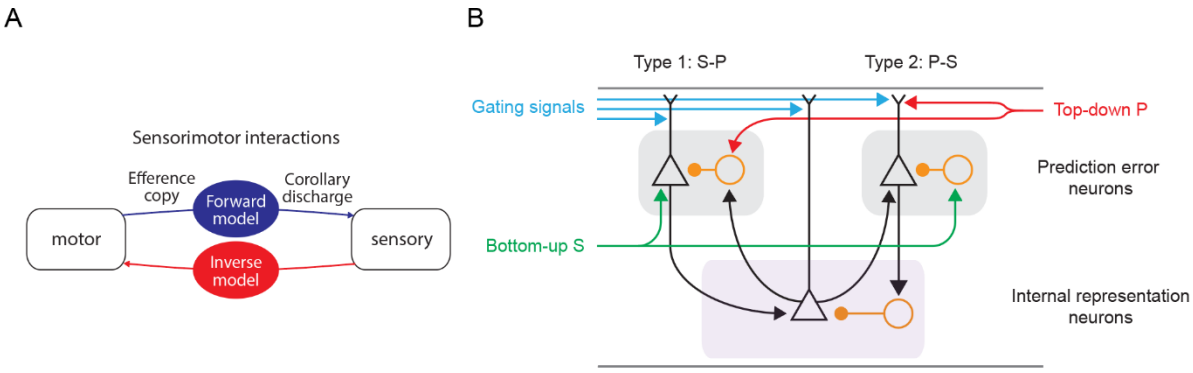

Figure 5. Predictive processing, adapted from (Keller and Mrsic-Flogel, 2018). **A:** To predict sensory consequences of self-generated movement, an efference copy is sent from motor areas to sensory areas. The transformation from a motor to sensory coordinate system is termed 'forward model' (given motor command copy, predict sensory input). An 'inverse model' refers to the mapping of sensory signals to motor commands (given an observation, what motor command explains it). **B:** Cortical circuit model, triangles represent excitatory neurons, circles represent inhibitory neurons. Given a prediction (P, top-right), prediction errors can arise in two ways: Left: More sensory input than expected (positive prediction error, S-P) or right: less sensory input than predicted (P-S, negative prediction error).

Sensory information is then shaped by the predictions, and determining which predictions best fit the sensory information is achieved by minimizing prediction errors of sensory consequences (Spratling, 2017). Internal models incorporate self and external features, and are thought to be used in two directions. Forward: What motor commands are necessary to achieve a sensory consequence, and inverse: what is the causal relationship between an action and a sensory consequence. When an agent engages in an action, a copy of the motor command (also called efference copy (von Holst and Mittelstaedt, 1950)) is sent to the forward model, which predicts sensory consequences of a movement. Importantly, this transformation may happen analogously between different sensory areas (Farrer et al., 2003). To illustrate, one area may code for geometric shapes, and the other for edges. If the internal representation for a square is active in the shape area, it will send 4 edges to the edge area, where the 4 edges will also be represented. The difference to the representational framework is how the representation is updated; in the representation framework this happens through bottom-up drive (feature detectors), and in predictive processing this happens through the comparison of bottom-up input and top-down predictions (based on internal representations) (Keller and Mrsic-Flogel, 2018). Early evidence for the predictive processing framework came not from new data, but from alternate explanations of existing observations, such as end-stopping (Rao and Ballard, 1999), where stimuli that extended over the classical receptive field of a neuron were suppressed and explained as a consequence of top-down inhibition. Another line of evidence comes from neural responses that are consistent with prediction errors (Attinger et al., 2017; Keller and Hahnloser, 2009; Keller et al., 2012; Saleem et al., 2013; Zmarz and Keller, 2016), prediction errors aligned to the retinotopic map of visual cortex (Zmarz and Keller, 2016), and motor-related signals from another cortical area to visual cortex, that are best explained as a prediction of visual flow (Leinweber et al., 2017).

Plasticity. We know from the field of computer science since ca. 1960, that to distinguish between object categories, it is sufficient to present a lot of learning data, and stepwise try to minimize the output between predicted and actual output throughout a network of connected nodes (Lillicrap et al., 2020). While algorithmic and implementation levels clearly are not comparable to biology (and differences are a subject of active research, reviewed here (Magee and Grienberger, 2020)), the overarching function, to reduce prediction errors, remains the same. Donald Hebb formalized a learning rule to explain how certain changes could be achieved on a biological level. Here, neurons would modify the connection strength (change of excitability; plasticity) as a function of pre- and postsynaptic activity (Hebb, 1949) and much evidence supports the notion that this is biologically implemented (Martin et al., 2000). It is less clear, how the synapses that should be updated are selected (Roelfsema and Holtmaat, 2018).

Glutamate receptors. In excitatory synapses, the amino acid glutamate is the most abundant neurotransmitter. Glutamate acts on a variety of metabotropic and ionotropic receptors. The latter are subdivided into three large families: N-methyl-D-aspartate (NMDA), α-amino-3-hydroxy-5-methyl-4-isoxazolepropionic acid (AMPA) and kainic acid (kainite) receptors, named after the chemical substances that were discovered to directly activate them *in vitro*. The main focus of this thesis is NMDA receptors, a conditional ion channel for calcium ions (Ca^{2+}) and sodium ions (Na^{+}), which have fascinated neuroscientists for decades because of their involvement in converting specific patterns of neuronal activity into lasting structural changes at the synapse.

NMDA receptors. NMDA receptors are glutamate-gated ion channels for calcium (Ca^{2+}) and sodium (Na^{+}) ions, present in many cells throughout the mouse brain (Lein, 2007; Monyer et al., 1994). It consists of 4 subunits (heterotetramer). Every subunit is coded for by a separate gene. *Grin1*, for example, codes for the GluN1 subunits and every NMDA receptor is thought consist of two GluN1 subunits. GluN1 subunits are expressed from E14 (day 14 of mouse embryonic development) until adulthood and a knockout of GluN1 receptors from birth is lethal (Forrest et al., 1994). The remaining subunits are either of type GluN2A-D or GluN3A-B subunits (reviewed in-depth here (Paoletti et al., 2013)). Subunit composition typically influences the temporal dynamics of the receptor; two GluN1 and two GluN2A subunit combinations, for example, deactivate faster than other subunit compositions. Adding to this diversity, each subunit also has multiple splice variants. During cortical development, a ratio-shift between GluN2A and GluN2B has been described, so that GluN2B subunits are partially replaced, a process which is thought to be activity dependent (Paoletti et al., 2013).

NMDA receptors have fascinated neuroscientists because of their ability to facilitate structural changes at synapses based on conditional firing of two connecting neurons. When the presynaptic neuron fires and releases glutamate, at first, the NMDA receptor remains closed; a Magnesium ion (Mg^{2+}) blocks the channel. Only when the postsynaptic membrane is depolarized (e.g., through a backpropagating action potential from the soma), with glutamate is present, and other co-ligands (glycine or D-serine) present, the NMDA receptor opens. The receptor also has several modulatory sites, sensitive to additional extracellular factors. Intracellularly, the receptor activates pathways involving inositol triphosphate (IP_3), guanylate kinase-associated protein (GKAP), postsynaptic density 95 (PSD95), and SH3 and multiple ankyrin repeat domains protein (SHANK) (Paoletti et al., 2013). Historically, NMDA receptors were thought to be located only at the post-synaptic neuron. However, they are also found at presynaptic sites, an area of active research (Bouvier et al., 2018).

CHAPTER I: VISUOMOTOR INTEGRATION AND VISUOMOTOR SKILL LEARNING DEPEND ON LOCAL PLASTICITY IN VISUAL CORTEX DURING DEVELOPMENT

Abstract. Visuomotor experience shapes responses in visual cortex during development. Coupling between motor output and visual feedback establishes a balance between top-down and bottom-up input that results in prediction error responses in layer 2/3 neurons. Whether local plasticity in visual cortex is necessary for the establishment of this balance is still unclear. Here, we probed the involvement of N-methyl-D-Aspartate (NMDA) receptor-dependent plasticity in mouse primary visual cortex (V1) during first visuomotor experience for the establishment of balance between top-down and bottom-up inputs. Using a conditional knockout of NMDA receptors as well as photoactivatable inhibition of CaMKII, we perturbed NMDA receptor-dependent plasticity in visual cortex. Using *in-vivo* two-photon calcium imaging, we found that NMDA receptors are essential during first development for visuomotor integration in V1, but not for maintenance later in adulthood. If this balance is disturbed even within one hemisphere during development, one hemisphere is enough to impact performance globally in a visually-guided navigation task. More generally, we characterized V1 activity in a state of local NMDA receptor dysfunction. These findings underline the importance of unimpaired NMDA receptor function during development and may help explain age-dependent characteristics in schizophrenia and anti-NMDA receptor encephalitis.

INTRODUCTION

The experience of coupling between movement and sensory feedback during development is necessary to learn to control and guide movement through sensory feedback. Raised without coupling between movements and visual feedback during visual development, kittens fail to use visual input to guide movements (Hein and Held, 1967; Held and Hein, 1963). The same coupling between locomotion and visual feedback is necessary to establish normal sensorimotor integration in visual cortex. Under normal conditions, visual cortex exhibits distinct responses to mismatches between movement and visual feedback in both humans and mice (Keller et al., 2012; Stanley and Miall, 2007; Zmarz and Keller, 2016). These mismatch responses can be interpreted as visuomotor prediction error signals (Keller and Mrsic-Flogel, 2018). In mice raised from birth, without coupling between movement and visual feedback, prediction error responses are absent and only emerge after first exposure to

normal visuomotor coupling (Attinger et al., 2017). Thus, the coupling between movement and visual feedback is essential for both visuomotor behavior and normal visuomotor integration in visual cortex. It is still unclear, however, where in the visual processing stream the plasticity occurs that is driven by experience with visuomotor coupling.

Given that visual cortex receives both the bottom-up visual input and signals consistent with a top-down prediction of visual feedback given movement (Leinweber et al., 2017) necessary to compute these mismatch responses, it has been speculated that visual cortex is a site of integration. In particular, it has been shown that neurons in layer 2/3 of visual cortex that are responsive to visuomotor mismatch, receive balanced and opposing top-down motor-related and bottom-up visual input (Jordan and Keller, 2020), consistent with a subtractive computation of visuomotor prediction errors. This is consistent with the interpretation that visuomotor experience establishes a balance between equal and opposing top-down and bottom-up input on individual layer 2/3 neurons. If this were so, we would predict that perturbing plasticity locally in V1 during visuomotor development should prevent the establishment of a normal balance between bottom-up and top-down inputs in V1, and consequently an impairment of visuomotor prediction errors in layer 2/3 visual cortex neurons.

Here, we tested this using two separate approaches to interfere with plasticity locally in V1 during first visuomotor experience. First, we used a local knockout of N-methyl-D-Aspartate (NMDA) receptors in visual cortex prior to first visuomotor experience. NMDA receptors are known to be involved in a wide variety of different forms of plasticity (Paoletti et al., 2013), and are necessary for activity-dependent synaptic strengthening in cortex (Hasan et al., 2013; Lo et al., 2013). In a parallel approach, we then used a photo-activatable inhibitor of the Ca2+/calmodulin-dependent protein kinase II (CaMKII), which allowed us to inhibit CaMKII in a cell-type specific manner. The function of CaMKII is tightly linked to NMDA receptors, and both are thought to be on the same synaptic plasticity pathway. We find that both types of manipulations systematically impair the development of normal visuomotor integration in layer 2/3 neurons, commensurate with the impairment observed in mice that are raised without experience of the coupling between movement and visual feedback (Attinger et al., 2017). Our results demonstrate that plasticity in V1 during first visual experience is necessary for the development of normal visuomotor integration.

RESULTS

NMDA receptor dependent plasticity in visual cortex is necessary for visuomotor integration.

To determine the dependence of visuomotor integration in visual cortex on local plasticity, we quantified the effect of a conditional knockout of NMDA receptors in visual cortex prior to first visual exposure on functional responses in L2/3 neurons of visual cortex. For this, we used $NR1^{flox}$ mice, which have a modified version of the *Grin1* gene (also referred to as *NMDAR1*, an essential subunit of the NMDA receptor) that is flanked by loxP sites (Tsien et al., 1996). We dark reared these mice from birth and injected a Cre-expressing adeno-associated viral vector (AAV2/1-EF1α-Cre-T2A-mCherry) unilaterally into visual cortex at postnatal day P21 prior to first visual exposure (Group 1: $\Delta Grin1_{juv}$; **Figures 1A and 1B**). At P30, we then injected a second AAV vector to express GCaMP6f (AAV2/1-EF1α-GcaMP6f) bilaterally in both visual cortices to record neuronal activity in a knockout hemisphere and a within animal control hemisphere. Mice were then exposed to visual input for the first time in their life at P32, when they were exposed to a virtual environment that provided closed loop feedback between forward locomotion and backward visual flow in a virtual corridor (Attinger et al., 2017). Mice were trained in this setup for 2 hours every other day for 12 days (6 sessions), after which we then measured calcium activity in layer 2/3 neuron using two-photon imaging (**Figure 1C**). To validate the method for the local knockout of *Grin1* expression with this approach, we used an mRNA in-situ hybridization against *Grin1* mRNA in a subset of mice (**Figure 1D**). During the calcium activity recording session, mice were first exposed to closed-loop visual flow feedback in a virtual corridor (see Methods). To measure mismatch responses, we introduced brief (1 s) halts of visual flow at random times (Keller et al., 2012). To estimate the contributions of visual flow and locomotion separately, mice then were presented with a playback of the visual flow they previously self-generated in the closed-loop session. We will refer to this as the open-loop session. To measure visual responses, mice were then presented with full-field drifting gratings of different orientations. Finally, to isolate motor-related signals, we also measured locomotion related activity in complete darkness. Note that we will operationally define mismatch responses as negative prediction errors and responses to visual gratings as positive prediction errors. The argument being that a mismatch constitutes less visual flow than predicted based on locomotion and visual flow history, while a sudden onset of a visual flow constitutes more visual flow than predicted.

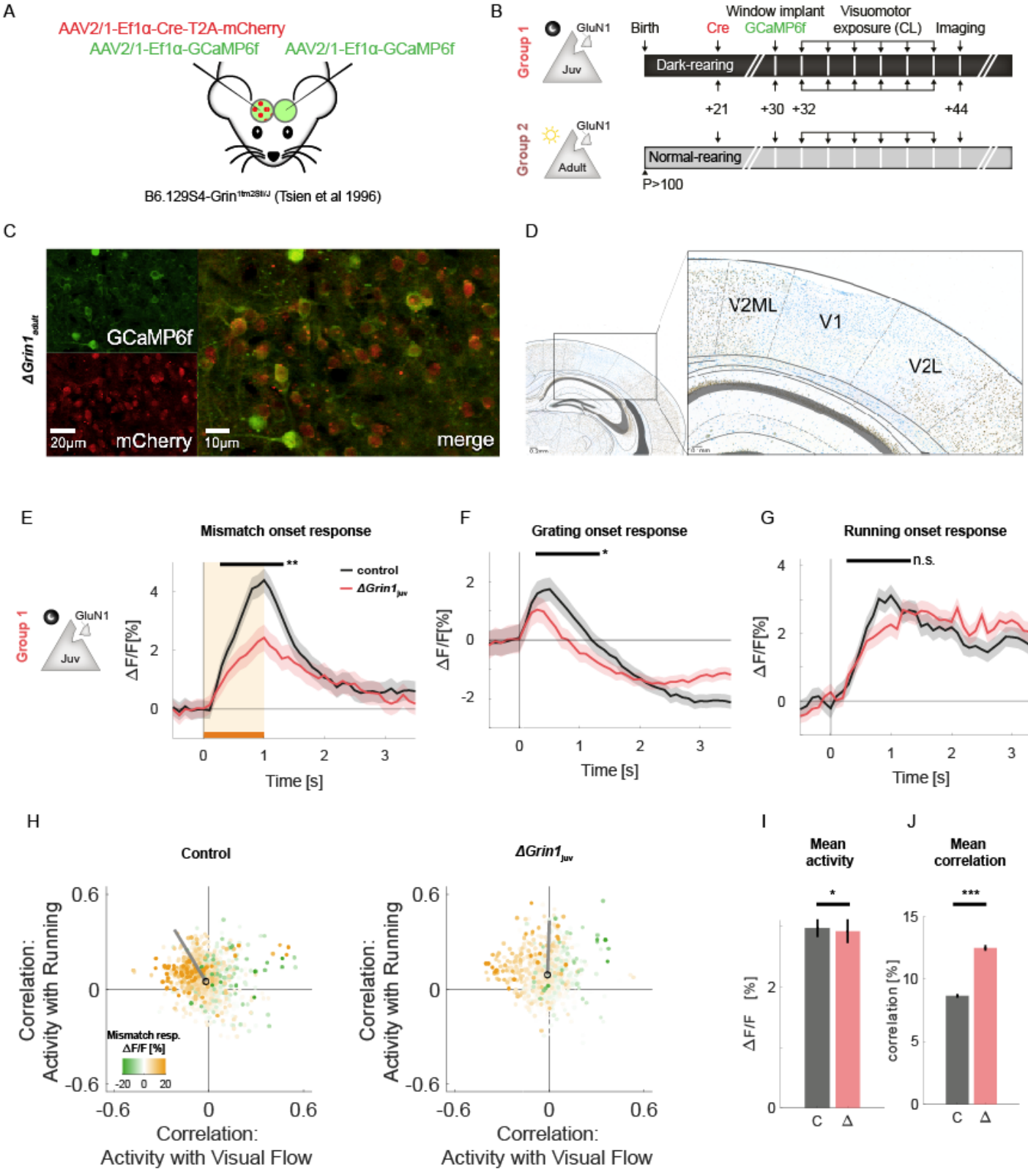
A
AAV2/1-Ef1α-Cre-T2A-mCherry
AAV2/1-Ef1α-GCaMP6f
AAV2/1-Ef1α-GCaMP6f
B6.129S4-Grin1tm2Stl/J (Tsien et al 1996)
B
Group 1
GluN1
Juv
Group 2
GluN1
Adult
Birth
Cre
Window implant
GCaMP6f
Visuomotor exposure (CL)
Imaging
Dark-rearing
+21
+30
+32
+44
Normal-rearing
P>100
C
ΔGrin1adult
GCaMP6f
mCherry
merge
20μm
10μm
D
V2ML
V1
V2L
E
Mismatch onset response
Group 1
GluN1
Juv
control
ΔGrin1juv
**
ΔF/F[%]
Time [s]
F
Grating onset response
*
ΔF/F[%]
Time [s]
G
Running onset response
n.s.
ΔF/F[%]
Time [s]
H
Control
ΔGrin1juv
Correlation: Activity with Running
Correlation: Activity with Visual Flow
Mismatch resp. ΔF/F [%]
I
Mean activity
*
ΔF/F [%]
C
Δ
J
Mean correlation
***
correlation [%]
C
Δ

Figure 1. Unimpaired NMDA receptor function is necessary for development of normal visual and mismatch responses.

(**A**) Experimental setup and injection schematic. We injected a Cre-expressing virus on the right hemisphere (effecting the *Grin1* knockout within ca. 10-12 days) and a calcium indicator (GCaMP6f) in both hemispheres.

(**B**) Experimental timeline. Mice were dark-reared from birth. AAV injections occurred at postnatal day 21 (P21, Cre) and P30 (GCaMP6f). Imaging window implantation occurred on P30. Mice had 6 training sessions in closed-loop condition (visuomotor exposure) before imaging at P44. Two groups of mice were imaged, one dark-reared (Group 1) and one adult, light-reared (Group 2).

(**C**) Example of expression pattern during *in-vivo* imaging. Left, top: Green-filtered channel demonstrating GCaMP6f expression. Left, bottom: Red-filtered channel demonstrating mCherry tag expression. Right: Merge of both channels.

(**D**) In-situ hybridization against *Grin1* mRNA (probe target region 2892-4127, see methods) confirming the local knockout of *Grin1* in visual cortex. Blue: Hematoxylin stain for cell nuclei, brown: hybridization signal. Brain regions were identified using a mouse brain atlas (Franklin and Paxinos, 2012).

(**E**) The average population response (ΔF/F) to mismatch was stronger in control (black) than in $\Delta Grin1_{juv}$ (red) hemispheres. Orange area and bar indicate duration of mismatch; shading indicates SEM. The mean response of every neuron in the indicated horizontal bar (top) is compared using the rank-sum test, with the following denotation for significance. *$p < 0.05$, **$p < 0.01$ ***$p < 0.001$.

(**F**) Same as (**E**) but for moving grating responses following a grey screen.

(**G**) Same as (**E**) but running onset in closed-loop sessions.

(**H**) Correlation coefficients between neural activity (ΔF/F) of layer 2/3 neurons with running speed and with visual flow in control (left) and $\Delta Grin1_{juv}$ (right) hemispheres during open-loop sessions. Each dot represents a single neuron. Dot color indicates the amplitude of the mismatch response (ΔF/F [%]). Black circles indicate the mean correlation values. The solid black line indicates the angle between the first principal component of the distribution and the y axis (see Methods). Shift in principle component angle is consistent with a lack of circuit maturation because of impaired plasticity.

(**I**) Mean activity of all recorded cells (C: neurons in control hemisphere, Δ: neurons in *Grin1* knock-out hemisphere) during closed-loop, error bars indicate SEM over neurons.

(**J**) Average pairwise correlation of neuronal activity is higher in *ΔGrin1* (red) compared to that in the control (black) hemisphere, consistent with a lack of diversification because of impaired plasticity.

We found that visuomotor mismatch responses in the knockout hemisphere were reduced compared to the control hemisphere and commensurate with that in mice that never experienced coupling between locomotion and backward visual flow (**Figures 1D-1E and S1A,** $p<0.05$ control, couple trained; $p<0.05$ $\Delta Grin1_{juv}$, non-coupled trained, rank-sum test). We also found a reduction of grating onset responses (**Figure 1E-1F**), but no evidence of a reduction of motor-related activity upon running onset in a closed loop environment (**Figure 1G**). The fact that mainly mismatch and visual responses are influenced by NMDA receptor knockout is consistent with impairment of the comparator function of layer 2/3 (Jordan and Keller, 2020). Mismatch responses are thought to arise from balanced and opposing bottom-up visual inhibitory input and top-down motor-related excitation. A reduction of mismatch responses could be the result of a reduction in top-down or bottom-up input, or a failure to match top-down excitation and bottom-up inhibition. To start to disambiguate these two possibilities, we estimated the net bottom-up visual input and the net top-down motor-related input by calculating the correlation of neuronal activity with visual flow and locomotion for each neuron (**Figure 1H**).

Consistent with responses in mice without an NMDA receptor knockout (Attinger et al., 2017), we found that in the control hemisphere neurons with high mismatch responses clustered in the quadrant of negative correlation with visual flow and positive correlation with running speed. In the knockout hemisphere, we found that both the average correlation with running speed and that with visual flow were increased relative to the control hemisphere (mean visual correlation control hemisphere: -0.017, $\Delta Grin1_{juv}$ hemisphere: -0.010, $p < 10^{-5}$; running correlation control hemisphere: 0.048, $\Delta Grin1_{juv}$ hemisphere: 0.090, $p < 10^{-5}$; rank-sum test), and the overall distribution resembled the one we had observed in previous work in mice raised without coupling between running and visual flow (Attinger et al., 2017). We quantified this using the angle of the first principal component of the distribution relative to the axis defined by the correlation with running. Similar to mice raised with coupling between running and visual flow, we found that in the control hemisphere the majority of neurons exhibited opposing correlation with running and visual flow, which manifested as a principal component close to the negative diagonal (control hemisphere: -29.8°, 95%-confidence interval (CI) = [-50.32, -13.63]; knockout hemisphere: 0.1°, CI = [-10.88, 10.63], bootstrap test with 10.000 redraws; compared to an angle in coupled trained animals: -16.74°, CI = [-4.16, -34.36], and in non-coupled trained animals: 36.58°, CI = [43.40, 29.63]; **Figure S1A-C**). This would be consistent with a failure to establish the necessary balance between top-down and bottom-up input, or a reduction in feed-forward visually driven inhibition. Given that mismatch and visual flow onset responses are reduced, this could simply be explained by an overall reduction in mean activity. We found that there was a reduction in mean activity, but this reduction was only 1.8% ($p < 0.012$, rank-sum test, **Figure 1I**) and cannot account for the reduction in mismatch responses.

Lastly, consistent with the effect of systemic inhibition of NMDA receptors on correlations of layer 2/3 neurons (**Figure S1d**)(Hamm et al., 2017), we found that in the knockout the average pairwise correlation of neuronal activity is higher compared to that in the control hemisphere ($p<10^{-5}$, rank-sum test, **Figure 1J**). Thus, NMDA receptor knockout prior to first visual exposure prevents the development of normal visuomotor prediction error responses in visual cortex. These results would be consistent with either a role of the NMDA receptor in the learning of visuomotor integration in visual cortex, or, alternatively, NMDA receptors might be necessary *per se* for normal calcium responses to mismatch and grating onsets. The latter could either be achieved by the NMDA receptor knockout rendering neurons less excitable, or by directly limiting the calcium response. To disambiguate this, we repeated the same experiments in a second group of mice that had been normally reared to adulthood with normal light-dark cycle (Group 2: $\Delta Grin1_{adult}$; **Figure 1B**). We found that in these animals there was no difference in the responses between those in the control hemisphere and those in the knockout hemisphere to any of the three stimuli (**Figures 2A-C**). Consistent with this, we also found that the distribution of visual flow and running correlations were similar between both hemispheres (**Figure 2D**). Though we found a reduction in overall activity in the knockout hemisphere compared to control, which is consistent with the finding that pharmacological inhibition of NMDA receptors in adult animals results in a decrease of V1 activity (Ranson et al., 2019) (**Figure 2E**). And similar to the effect in juvenile knockout, we also saw an increase in the average correlation between neurons (**Figure 2F**). Thus, NMDA receptors are necessary for the normal development of prediction error responses in visual cortex, but not necessary to maintain these responses when visual cortex is fully trained by experience.

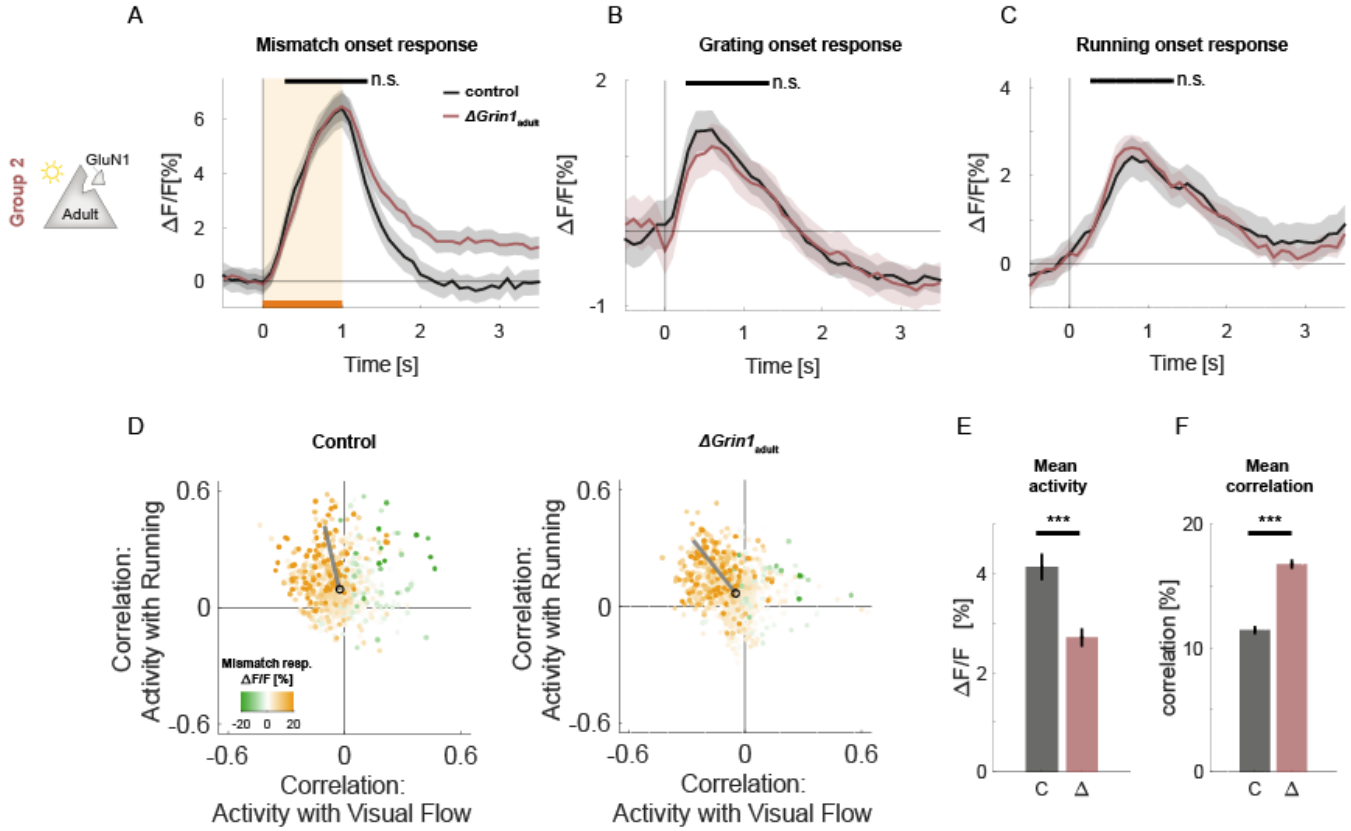

561 **Figure 2. NMDA receptor knockout in the adult mouse does not change visual or visuomotor**
562 **responses.**

563 (**A**) The average population response (ΔF/F) to mismatch was similar in control (black) and *ΔGrin1*$_{adult}$
564 (red) hemispheres. Orange area and bar indicate duration of mismatch; shading indicates SEM. The
565 mean response of every neuron in the indicated horizontal bar (top) is compared using the rank-sum
566 test, with the following denotation for significance. *p < 0.05, **p < 0.01 ***p < 0.001.

567 (**B**) Same as (**A**) but for moving-grating responses following a grey screen.

568 (**C**) Same as (**A**) but running onset in closed-loop sessions.

569 (**D**) Correlation coefficients between neuronal activity (ΔF/F) of layer 2/3 neurons with running speed
570 and with visual flow in control (left) and *ΔGrin1*$_{adult}$ (right) hemispheres during open-loop sessions.
571 Each dot represents a single neuron. Dot color indicates the amplitude of the mismatch response (ΔF/F
572 [%]). Black circles indicate the mean correlation values. The solid black line indicates the angle
573 between the first principal component of the distribution and the y-axis (see Methods).

574 (**E**) Mean activity of all recorded cells (C: neurons in control hemisphere, Δ: neurons in *Grin1* knock-
575 out hemisphere) during closed-loop, error bars indicate SEM over neurons.

576 (**F**) Average pairwise correlation of neuronal activity in *ΔGrin1* (red) compared to that in the control
577 (black) hemisphere.

Given the observed deficit in the development of prediction error responses induced by the NMDA knockout, we would also expect a similar deficit in the suppression of predictable responses. To investigate this, we looked at the suppression of running onset responses by visual flow in the closed-loop condition. A running onset in the closed-loop condition is typically associated with an increase in activity that is transient (**Figure 3A**). Comparing this to running onsets in darkness, we find that the initial increase is similar, but the responses do not decrease over time. One interpretation of this is that the visual flow coupled to locomotion in the closed-loop condition triggers a suppression of the running-related responses. Note, if one were to assume layer 2/3 neurons exclusively signal prediction errors, one would expect no running onset responses in a closed-loop condition at all. The fact that we see transient onset response could be explained either by technical limitations in our virtual reality system that introduces a lag between running and visual flow, or by a lack of precision in top-down predictions. We quantified the suppression in this running-onset response in closed-loop condition by taking the difference between the running onset activity in darkness and that in the closed-loop condition (**Figure 3A**). Computing this difference for control mice, the *ΔGrin1*$_{juv}$ mice, and *ΔGrin1*$_{adult}$ mice, we found that this suppression was absent only in the knockout hemisphere of the *ΔGrin1*$_{juv}$ mice (**Figure 3B, C**). In sum, we find that the NMDA receptors are critical for the establishment of normal visuomotor integration during first visuomotor experience.

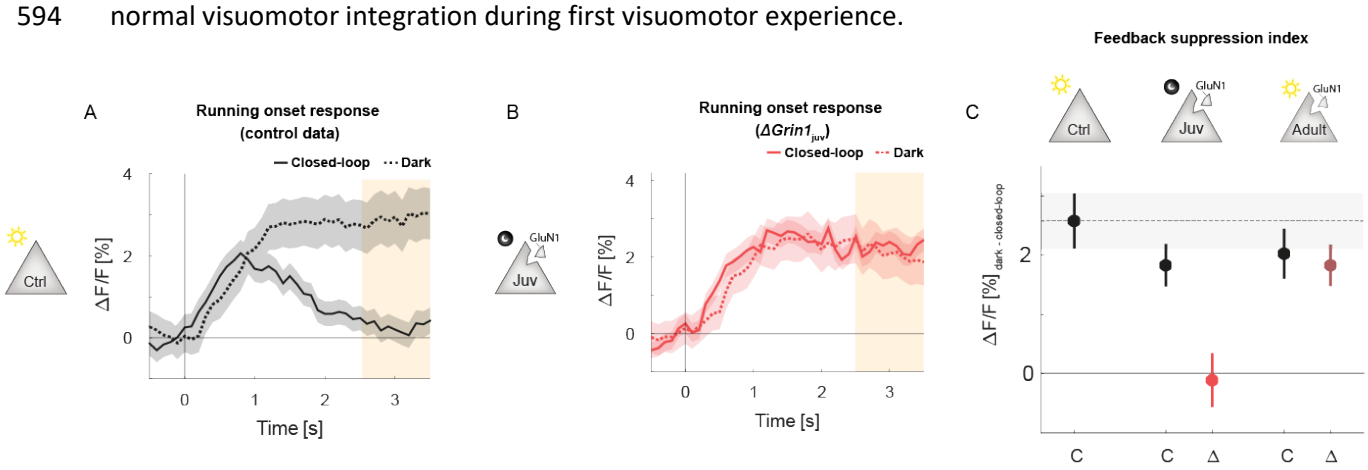

Figure 3. Suppression of predictable visual flow is reduced in mice with *ΔGrin1* prior to first visual experience.

(**A**) The average population response (ΔF/F) to running onset in closed-loop sessions (solid) and dark sessions (dotted) in adult control animals. Orange area indicates duration of subtraction window (dark – closed-loop). Shading indicates SEM over neurons.

(**B**) Same as (**A**) but for *ΔGrin1*$_{juv}$.

(**C**) Quantification of suppression of predictable visual flow. The feedback suppression index is calculated as difference of average late (2.5-3.5s) running-onset response in dark and closed-loop condition (dark$_{late}$ - closed-loop$_{late}$). Error bars indicate SEM over neurons. C: neurons in control hemisphere, Δ: neurons in *Grin1* knock-out hemisphere.

Local NMDA receptor dysfunction during development leads to impaired visuomotor skill learning later in life.

Assuming developmental plasticity in visual cortex is necessary for the establishment of normal visuomotor integration in visual cortex, we would expect that the *ΔGrin1*$_{juv}$ mice would exhibit behavioral impairments in cortex dependent visuomotor tasks. To test this, we trained these mice in a visuomotor task later in life. The experimental group of mice was composed of 6 *ΔGrin1*$_{juv}$ mice. For these experiments we used two control groups. The first of was 13 *ΔGrin1*$_{adult}$ mice. The second group was composed of 6 control mice (group Control$_{juv}$) that did not receive a *Grin1* knockout but were dark-reared from birth. The *ΔGrin1*$_{juv}$ and Control$_{juv}$ groups were dark-reared until P32 and all three groups were initially exposed to closed-loop experience in a virtual reality setup as described above and subsequently trained to perform a virtual navigation task (Heindorf et al., 2018) (**Figures 4A, B**). In this task, mice had control over movement in a virtual 2D-corridor through rotation and forward locomotion on a spherical treadmill. They had incentive to reach the end of the virtual corridor for a water reward. Training lasted for 7 days, with an hour-long session each day. We quantified performance using an index that is based on the fraction of distance traveled toward the target normalized by the total distance travelled (see Methods). The dark-reared control mice of the Control$_{juv}$ group and the adult knockout group *ΔGrin1*$_{adult}$ both learned to perform the task over the course of the training (early vs. late: $p < 0.05$, $p < 0.05$, respectively; rank-sum test). The *ΔGrin1*$_{juv}$ mice, however, failed to show any evidence of increased performance over the 7 days (early vs. late: $p > 0.05$; rank-sum test), and exhibited significantly reduced performance compared to the two control groups ($p < 0.05$, and $p < 0.05$, respectively; rank-sum test; **Figure 4C**). To test for the mice's ability to trigger a behavioral response to an unexpected perturbation of visual feedback, we had introduced sudden offsets of the current heading at random times by 30° to the left or to the right. With training, mice learn to correct for these offset perturbations with a turn in the virtual reality that corrects for the offset. Again, both Control$_{juv}$ and *ΔGrin1*$_{adult}$ mice corrected for offset perturbations with a compensatory turn in the correct direction by the end of training (**Figure 4D**). The *ΔGrin1*$_{juv}$ mice failed to correct even late in training. Interestingly, they exhibited a trend for an asymmetry in exhibiting a slightly increased correction when the perturbation was in the direction of the visual hemifield seen by the control hemisphere that had not received an NMDA receptor knockout (**Figure 4D**). Quantifying this as the learning-related change in offset perturbation response, we find that Control$_{juv}$ and *ΔGrin1*$_{adult}$ mice exhibit larger learning related changes than the *ΔGrin1*$_{juv}$ mice (**Figure 4E**). Thus, consistent with the dependence of normal visuomotor integration on NMDA receptors during first visuomotor experience, we find that mice that lack NMDA receptors during first visuomotor experience are impaired in learning certain visually guided motor tasks later in life.

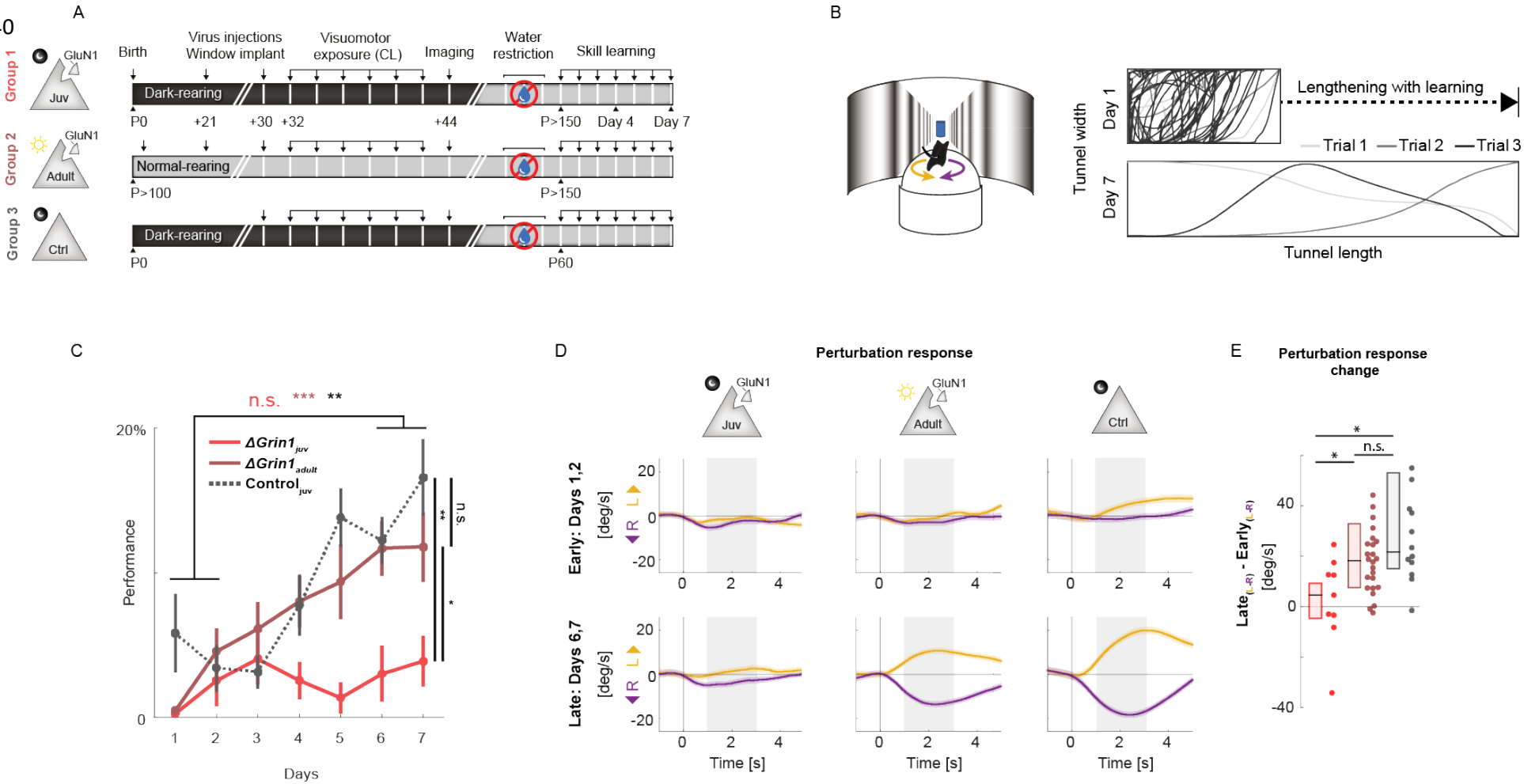
A
Group 1
GluN1
Juv
Group 2
GluN1
Adult
Group 3
Ctrl
Birth
Virus injections
Window implant
Visuomotor
exposure (CL)
Imaging
Water
restriction
Skill learning
Dark-rearing
P0
+21
+30
+32
+44
P>150
Day 4
Day 7
Normal-rearing
P>100
P>150
Dark-rearing
P0
P60
B
Tunnel width
Day 1
Day 7
Lengthening with learning
Trial 1
Trial 2
Trial 3
Tunnel length
C
n.s.
***
**
20%
0
Performance
ΔGrin1juv
ΔGrin1adult
Controljuv
1
2
3
4
5
6
7
Days
n.s.
**
*
D
Perturbation response
GluN1
Juv
GluN1
Adult
Ctrl
Early: Days 1,2
Late: Days 6,7
[deg/s]
20
0
-20
L
R
0
2
4
Time [s]
E
Perturbation response change
Late(L-R) - Early(L-R)
[deg/s]
40
0
-40
*
*
n.s.

Figure 4. NMDA receptors in visual cortex are necessary during first visuomotor experience to enable learning of a visuomotor task later in life.

(**A**) Experimental approach and timeline. Three groups of mice were used: Group 1: $\Delta Grin1_{juv}$, Group 2: $\Delta Grin1_{adult}$ and Group 3: dark-reared control animals, either after imaging (Group 1, 2) or after training (Group 3). After this, mice were water restricted and entered the skill learning paradigm.

(**B**) Left: Schematic of virtual-reality task. Mice have control of forward motion and rotation in a virtual 2D-corridor, and are trained navigate to the end of the corridor for a water reward. As performance increased, the task difficulty was increased by lengthening the virtual corridor. Right: Schematic top-down view of a corridor on day 1 (short, top) and day 7 (long, bottom), with three trials of the mouse shown as different grey-level lines.

(**C**) Task performance as a function of training day (see Methods) of mice (red) , (dark red), and dark-reared control (black, dotted) mouse groups over 7 days.

(**D**) Turning behavior of $\Delta Grin1_{juv}$, $\Delta Grin1_{adult}$ and dark-reared control mouse groups. Top: day 1 and 2, bottom: day 6 and 7. Grey shading indicates time selected for quantification (see F). Shading indicates SEM over trials. Note, in $\Delta Grin1_{juv}$ and $\Delta Grin1_{adult}$ mice, the knockout hemisphere is right.

(**E**) Quantification of (D) with boxes indicating the lower and upper quartiles and the line indicating the median, next to it the actual data points (* indicates $p<0.05$, rank-sum test). Perturbation response change was calculated for every mouse as follows: $mean_{(left\ turn)}$ - $mean_{(right\ turn)}$ on $day_{(6\ to\ 7)}$ – the same on $day_{(1\text{-}2)}$.

CaMKII-dependent plasticity in SST interneurons is necessary for feed-forward visual inhibition.

A central circuit element in the computation of prediction error responses are inhibitory interneurons that allow for a subtraction of a bottom-up sensory input and a top-down prediction (Keller and Mrsic-Flogel, 2018), and could establish the observed opposing influence of visual and locomotion-related input observed in layer 2/3 neurons (Jordan and Keller, 2020). Based on measurements of calcium responses to visuomotor mismatches and artificial manipulations of activity, we have previously speculated that a subset of somatostatin (SST) positive interneurons mediate the visually driven inhibition necessary for negative prediction error responses in layer 2/3 excitatory neurons (Attinger et al., 2017). Thus, we set out to test whether an impairment of plasticity selectively in SST interneurons in visual cortex during first visuomotor experience would result in a failure to establish visually driven inhibition in layer 2/3 neurons as predicted. To do this, we turned to a method that would allow us to target the intervention to SST neurons selectively in visual cortex without the need for an intersectional approach using multiple recombinases. We used a method to inhibit Calcium/calmodulin-dependent kinase II (CaMKII) using a photoactivatable autocamtide inhibitory peptide 2 (paAIP2) (Murakoshi et al., 2017). CaMKII has been shown to be an essential element of NMDA receptor dependent plasticity (Barria and Malinow, 2005; Gambrill and Barria, 2011; Wang et al., 2011). NMDA receptor subunits are known to immunoprecipitate with CaMKII, and the formation of the CaMKII–NMDA receptor complex is thought to have a key role in learning (Lisman et al., 2012).

We repeated the experiments we performed with the NMDA receptor knockout using paAIP2 in three groups of mice to target CaMKII inhibition either to excitatory neurons, SST interneurons, or parvalbumin (PV) positive interneurons. All mice were dark reared from birth (**Figure 5B**). The first group consisted of 6 wild-type mice that received an injection of an AAV to express paAIP2 under a CaMKIIα-promotor (AAV2/1- CaMKIIα-mEGFP-P2A-paAIP2) in right visual cortex. The other two groups consisted of 7 SST-Cre and 6 PV-Cre mice that each received an injection of (AAV2/1- DIO-mEGFP-P2A-paAIP2P) in right visual cortex. At P30, prior to first visuomotor experience mice then received an injection of an AAV to express a red-shifted calcium indicator (AAV2/1- Ef1α-NES-jRGECO1a) in both left and right visual cortex (**Figure 5A**). All mice were then exposed to a virtual environment that provided coupling between forward locomotion and backward visual flow for 2 hours once every 2 days, for 12 days and were dark housed otherwise. To activate paAIP2 while mice were on the virtual reality setup, we illuminated visual cortex bilaterally using a blue (473nm) laser through the glass windows implanted for subsequent two-photon imaging (see Methods). We then proceeded to again measure mismatch responses, visual responses, as well as running onset responses in layer 2/3 neurons. Similar to the responses in *ΔGrin1*$_{juv}$, we found that the strongest response changes were present in mismatch and visual responses, and less so in running onset

responses (**Figures 5D-F**). Mismatch responses were again reduced in the inhibited hemisphere compared to the control hemisphere. Intriguingly, the CaMKII inhibition resulted in a massive increase in visually driven activity of layer 2/3 neurons. It is important to note that our within animal control suffers from the confound that the two hemispheres are directly connected. For instance, the fact that visual response are also massively increased in the control hemisphere relative to control responses (see **Figure 5E**, or (Attinger et al., 2017)), is likely caused by this direct interaction. A similar problem befalls our experiments using the NMDA receptor knockout. However, given that the effect sizes were considerably smaller in those experiments, cross-talk effects are likely also less apparent. A potential explanation for this increase in visually driven responses lies in the fact that there is a systematic asymmetry regarding cortical depth. We are using light applied to the surface of the brain to activate the paAIP2. Light power falls off exponentially with cortical depth (**Figure S2B**), with an estimated half-length of 37µm, comparable to previous research (Yona et al., 2016). This, combined with the fact that CaMKII expression is higher in superficial layer 2/3 neurons than layer IV and V in the mouse (Lein, 2007), could result in an increased effect of the CaMKII inhibition in superficial synapses. Long-range cortical input, which is thought to carry motor-related input to V1 (Leinweber et al., 2017), arrives preferentially on more superficial inputs than the bottom-up visual input (Young et al., 2021). Thus, our CaMKII inhibition likely preferentially blocks plasticity in top-down inputs. Consistent with the NMDA receptor knockout, we also found an increase in the average correlation of activity between neurons (**Figure S2B**).

Inhibiting CaMKII in SST positive interneurons had a similar effect on mismatch and visual responses as in excitatory neurons, decreasing the former and increasing the latter (**Figure 5HI**). However, consistent with the idea that SST neurons are central to mediating visually driven inhibition, we found a strong increase in the average correlation of neuronal activity with visual flow, as measured during open-loop condition (**Figure 5J**). This was markedly different from the strong increase in negative correlation with visual flow resulting from inhibiting CaMKII in excitatory neurons (**Figure 5G**). This increase in visual flow correlation was not simply the consequence of reducing inhibitory input as it was absent when we repeated the same analysis for animals that had received inhibition of CaMKII in PV positive interneurons. On comparing the average visual flow correlation across all manipulations, we find that only the inhibition of CaMKII in SST interneurons resulted in a net positive correlation with visual flow (**Figure 5G**). All paAIP2 inhibition induced differences reverted back to control response over the course a few days of normal visuomotor coupling (**Figure S3**). Together, these data are be consistent with the interpretation that interfering with plasticity in the top-down input to layer 2/3 as well as the visually driven inhibition mediated by SST neurons results in a decrease of mismatch responses, albeit for different reasons.

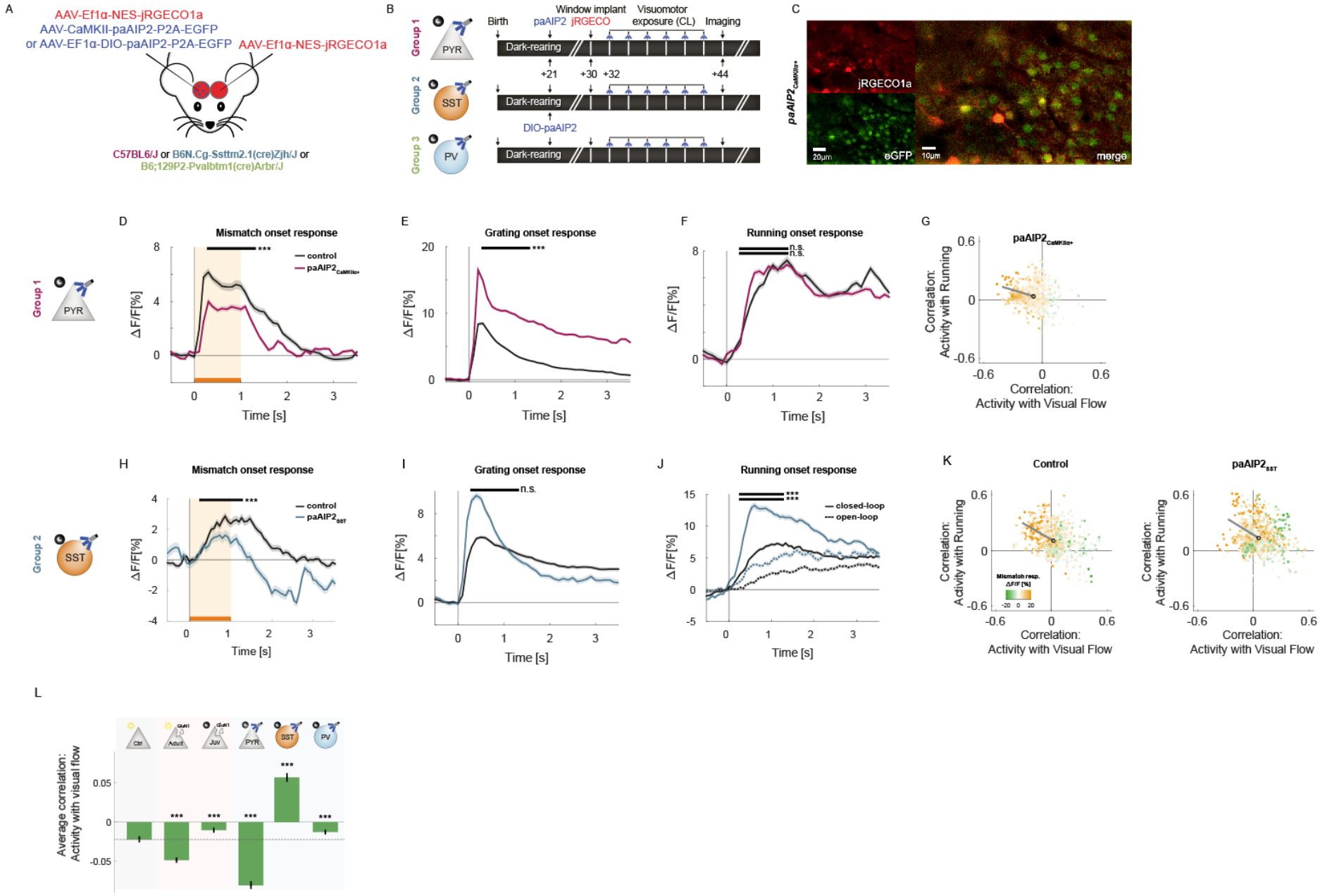
A
AAV-Ef1α-NES-jRGECO1a
AAV-CaMKII-paAIP2-P2A-EGFP
or AAV-EF1α-DIO-paAIP2-P2A-EGFP
AAV-Ef1α-NES-jRGECO1a
C57BL6/J or B6N.Cg-Ssttm2.1(cre)Zjh/J or
B6;129P2-Pvalbtm1(cre)Arbr/J
B
Group 1
Group 2
Group 3
PYR
SST
PV
Birth
Window implant
paAIP2 jRGECO
Visuomotor
exposure (CL)
Imaging
Dark-rearing
+21
+30 +32
+44
DIO-paAIP2
C
paAIP2CaMKIIα+
jRGECO1a
20μm
eGFP
10μm
merge
D
Mismatch onset response
control
paAIP2CaMKIIα+
ΔF/F[%]
Time [s]
E
Grating onset response
F
Running onset response
n.s.
G
paAIP2CaMKIIα+
Correlation:
Activity with Running
Correlation:
Activity with Visual Flow
H
Mismatch onset response
paAIP2SST
I
Grating onset response
J
Running onset response
closed-loop
open-loop
K
Control
paAIP2SST
Mismatch resp.
ΔF/F [%]
L
Ctrl
Adult
Juv
Average correlation:
Activity with visual flow

Figure 5. Blocking CaMKII in superficial synapses during first visuomotor experience increases bottom-up visual drive and reduces mismatch responses.

(**A**) Experimental setup and injection schematic. We injected a GFP-tagged paAIP2 or DIO-paAIP2 expressing virus on the right hemisphere and a calcium indicator (jRGECO1a) in both hemispheres.

(**B**) Experimental timeline. All mice were dark-reared from birth. AAV injections occurred at postnatal day 21 (P21, paAIP2 or DIO-paAIP2) and P30 (jRGECO1a). Imaging window implantation occurred on P30. Mice had 6 training sessions in closed-loop condition (visuomotor exposure) while we inhibited CaMKII optogenetically using a blue laser (473nm), before imaging at P44. We imaged three groups of mice: Group 1: Inhibition of CaMKII in CaMKIIα-positive neurons, targeted by viral promotor. Group 2: Inhibition of CaMKII in SST interneurons, targeted by DIO-paAIP2 construct and a Cre-expressing mouse line. Group 3: same as group 2, but for PV interneurons.

(**C**) Example of expression pattern during *in-vivo* imaging. Left, top: Red-filtered channel demonstrating jRGECO1a expression. Left, bottom: Green channel demonstrating mGFP tag expression. Right: Merge of both channels.

(**D**) The average population response (ΔF/F) to mismatch was stronger in control (black) than in paAIP2$_{CaMKII\alpha+}$ (purple) hemispheres. Orange area and bar indicate duration of mismatch, starting at time = 0s; shading indicates SEM. The mean response of every neuron in the indicated horizontal bar (top) is compared using the rank-sum test, with the following denotation for significance. *p < 0.05, **p < 0.01 ***p < 0.001.

(**E**) Same as (**D**) but for moving-grating responses following a grey screen.

(**F**) Same as (**D**) but running- onset in closed-loop sessions.

(**G**) Correlation coefficients between neuronal activity (ΔF/F) of layer 2/3 neurons with running speed and visual flow in paAIP2$_{CaMKII\alpha+}$ hemisphere during open-loop sessions. Each dot represents a single neuron. Dot color indicates the amplitude of the mismatch response (ΔF/F [%]). Black circles indicate the mean correlation values. The solid black line indicates the angle between the first principal component of the distribution and the y-axis (see Methods).

(**H**) Same as (**D**) but for inhibition of paAIP2$_{SST}$ group (inhibition in SST neurons, imaging activity in EF1α positive-neurons).

(**I**) Same as (**H**) but running-onset in closed-loop sessions.

(**J**) Same as (**H**), but for control and paAIP2$_{SST}$ hemispheres. Solid: Running onset responses in closed-loop sessions. Dotted: Running onset responses in dark sessions.

(**K**) same as in (G), but on inhibition of CaMKII using paAIP2 in SST neurons(right), or only control blue light stimulation (left).

(**L**) Mean correlation coefficients between neuronal activity (ΔF/F) of layer 2/3 neurons with visual flow in adult control animals and *ΔGrin1*$_{adult}$, *ΔGrin1*$_{juv}$, paAIP2$_{CaMKII\alpha}$, paAIP2$_{SST}$ and paAIP2$_{PV}$ knockout, resp. paAIP2 hemisphere.

DISCUSSION

Our results demonstrate that early in the life of a mouse, exposure to visuomotor coupling establishes a circuit in V1 capable of integrating motor and visual signals that enables visuomotor skill learning later in life. Given the block of NMDA receptor-dependent plasticity resulted in a reduction of responses in layer 2/3 neurons to mismatch and visual stimuli, we speculate that the impaired visuomotor skill learning is the consequence of a reduced capacity to compute visuomotor prediction errors. It has been shown that layer 2/3 neurons balance opposing bottom-up and top-down input to compute prediction errors (Jordan and Keller, 2020). Our results indicate that this balance is established by local plasticity in V1 through experience with visuomotor coupling. Given that when preventing this process from occurring in V1 impairs the ability of the mice to learn visuomotor tasks later in life, we hypothesize that ability of V1 to compute visuomotor prediction is an essential component of the computational strategy the brain uses to guide movement by visual feedback in more complex behavioral tasks.

Our strategy to knockout NMDA receptors in visual cortex is not specific to L2/3 neurons, and it is not certain if the effects we see in L2/3 neurons are the direct consequence of the NMDA receptor knockout in these neurons or a consequence of an effect in one of the other layers. What we do know, however, is that visual responses in the main source of bottom-up visual input to L2/3 neurons, layer 4 (L4), are less dependent on NMDA receptor function. A cortex-wide *Grin1* knockout in L4 neurons does not alter visually evoked potentials in visual cortex, nor does it impair visual acuity of the mice, both when the knockout is congenital or post-adolescent (Fong et al., 2020; Sawtell et al., 2003). Thus, we speculate that the NMDA knockout effects we observe are at least partially driven by interfering with establishing a normal input circuit to the L2/3 neurons.

NMDA receptors are thought to exert their influence on synaptic plasticity by increasing Ca2+ influx into the cell, where calmodulin binds Ca2+ and activates CaMKII. Consistent with the idea that CaMKII is one of the downstream molecules in NMDA receptor-mediated signaling, NMDA receptor activation triggered plasticity can be blocked by blocking CaMKII (Herring and Nicoll, 2016). In addition to this, activated CaMKII and NMDA receptors have been shown to directly interact (Leonard et al., 1999) to integrate learning related synaptic changes (Lisman et al., 2012). Thus, we would expect the NMDA receptor knockout and the chronic CaMKII inhibition to have similar effects on the responses of L2/3 neurons. While both manipulations resulted in reduced mismatch responses and left running related responses largely unchanged, the two had opposing effects on visual responses. Knockout of NMDA receptors in excitatory neurons resulted in a decrease in visual response in L2/3, while CaMKII inhibition resulted in a massive increase in bottom-up visual drive. It is possible that this discrepancy is the consequence of a difference in the extent of the inhibition of NMDA receptor-dependent

plasticity in L2/3 neurons. With the knockout strategy, one could expect a homogenous absence of NMDA receptors, whereas the CaMKII inhibition possibly has a heterogenous effect, with the inhibition of plasticity skewed more towards superficial synapses. The depth-dependent decrease in light intensity and thus effectiveness of paAIP2-mediated inhibition of CaMKII, coupled with a possible compensatory increase in visual responses in L2/3 due to higher expression of CaMKII in superficial layers compared to L4, could possibly account for the observed increase in visual response in paAIP2-mediated CaMKII inhibition data. Further L2/3 neurons likely receive bottom-up visual input predominantly on basal dendrites (Park et al., 2019), while motor-related top-down input that predominantly arrives in L1 (Leinweber et al., 2017) likely synapses more superficially on apical dendrites (Petreanu et al., 2009). Thus, we speculate that the CaMKII inhibition results in a differential impairment of plasticity in top-down and bottom-up pathways. Our data could be explained by assuming that the CaMKII inhibition blocks plasticity preferentially in top-down synapses, which in turn could result in a runaway increase of the strength of bottom-up input. Why this occurs, or what the learning rules are that drive this plasticity, is still unclear. Inhibiting CaMKII in somatostatin (SST)-expressing interneurons had a similar effect on mismatch and visual responses in excitatory neurons, and initially showed an increase in neural activity with both visual flow and running (**Figure 5I-J**). Whereas the CaMKII inhibition in CaMKIIα-positive cells left visual cortex L2/3 population mostly unchanged in terms of their correlation in open-loop sessions, of CaMKII inhibition in SST neurons led to the visual cortex L2/3 remarkably more responsive to both visual flow and running. Because this positive correlation changed within a short period of time (after ca 1h of visual exposure without CaMKII inhibition, **Figure 5**) to a state that is consistent with typical physiological correlation of similarly aged animals (**Figure 1H** and (Attinger et al., 2017)), and the control hemisphere (**Figure S2H**), it seems likely that CaMKII in SST neurons can profoundly shape activity correlation of pyramidal neurons during development. Interestingly, we did not find similar changes when we inhibited CaMKII in PV-expressing neurons (**Figure 5G and S3I**).

Our measurement is based on a calcium signal, and disruption of NMDA receptor function may introduce a confound in our data. The main determinant of somatic calcium signals are thought to be voltage-gated calcium channels (VGCCs) (Grienberger and Konnerth, 2012). NMDA receptors are the main source of calcium in dendritic spines (Sabatini et al., 2002). Suprathreshold stimuli produce additional Ca^{2+} influx through VGCCs, opened by backpropagating action potentials. Because our main effects are decreases of activity, and we measured our results with a calcium indicator, this could confound our results. We checked for changes in mean activity and found that the average activity was unchanged during closed-loop in $\Delta Grin1_{juv}$ data, suggesting that NMDA receptor mediated

836 calcium influx might only be a minor confound in juvenile mice. Compensatory mechanisms may also
837 play a role, as we see a decrease in *ΔGrin1*$_{adult}$ data.

838 Activation of NMDA receptors on pyramidal neurons is capable of potentiating inhibitory synapses in
839 cortex. Notably, this form of plasticity is specific to inputs from SST neurons and does not seem to
840 occur for inputs from PV or VIP neurons (Chiu et al., 2018). Furthermore, it has been suggested that
841 an NMDA receptor-dependent mechanism underlies inhibitory synapse development (Gu et al., 2016).
842 It is conceivable, that inhibitory synapses onto negative prediction error neurons do not fully form
843 during development of visual cortex if NMDA receptors are knocked out.

844 **Abbreviations**

845 **SEM** - Standard error of the mean

846 **NMDA** - N-Methyl-D-aspartate

847 **CaMKII** – Ca^{2+}/calmodulin-dependent protein kinase II

848 **paAIP2** - photo-activatable autocamtide 2 peptide, an inhibitor of CaMKII

849

850

851

SUPPLEMENTARY FIGURES

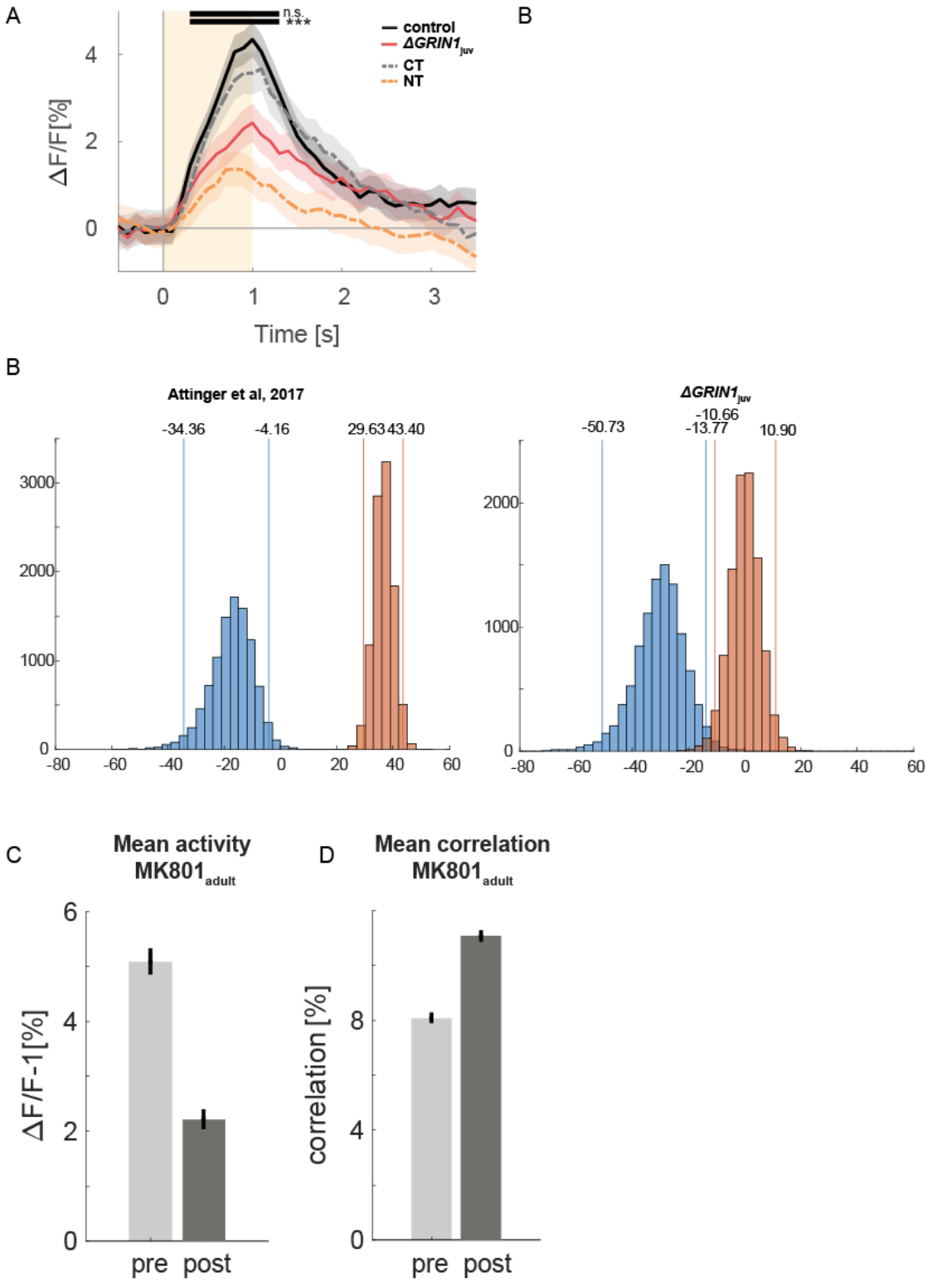

Figure S1. Comparison Attinger et al 2017.

(**A**) Mean population response on mismatch, current experiment, with coupled-trained and non-coupled trained data from Attinger et al.

(**B**) Bootstrap histogram of principal component angle from correlational analysis of activity with running speed and visual flow, for *ΔGrin1*$_{juv}$ data (right) and previous publication (left, Attinger et al., 2017), CT, control hemisphere: blue. NT, knockout hemisphere: red.

(**C**) Mean activity pre and 1h post MK801 injection (i.p., 0.1mg/kg); the activity was significantly lower post MK801 injection ($p<0.05$, rank-sum test).

(**D**) Mean correlation of every neuron with every other neuron. Neuron correlations were significantly increased post MK801 injection ($p<0.05$, rank-sum test).

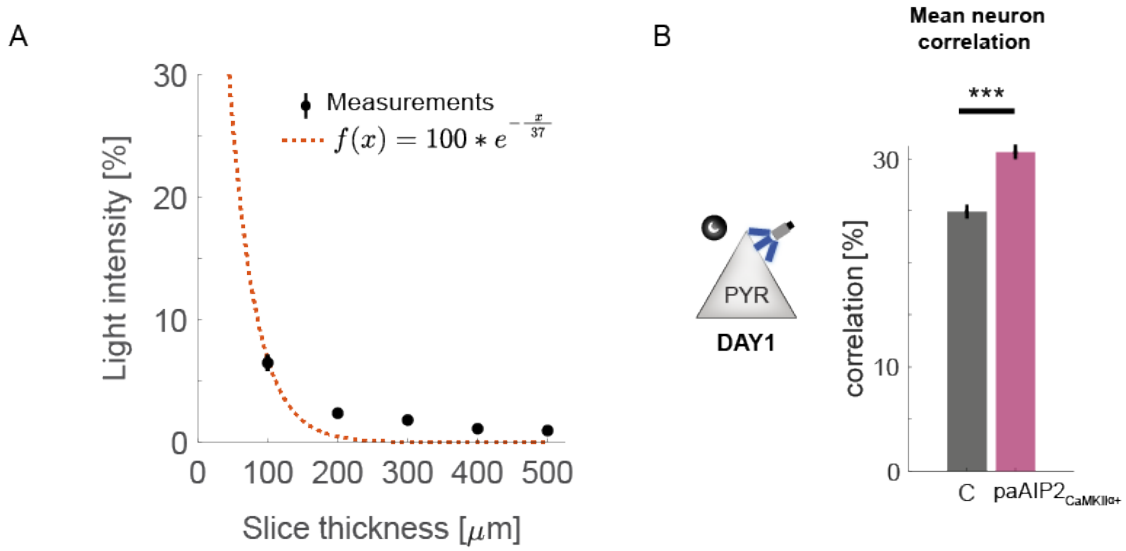

Figure S2. Additional CaMKII data, related to Figure 5.

(**A**) One-exponent fit (red dotted line) for blue laser (473nm) power attenuation through different thicknesses of brain tissue (coronal slices). 5 slices were measured 3 times in random sequence, the error bar denotes SEM.

(**B**) Mean correlation of every neuron with all other neurons during closed-loop. C: neurons in control hemisphere, Δ: neurons in paAIP2$_{CaMKII\alpha+}$ hemisphere

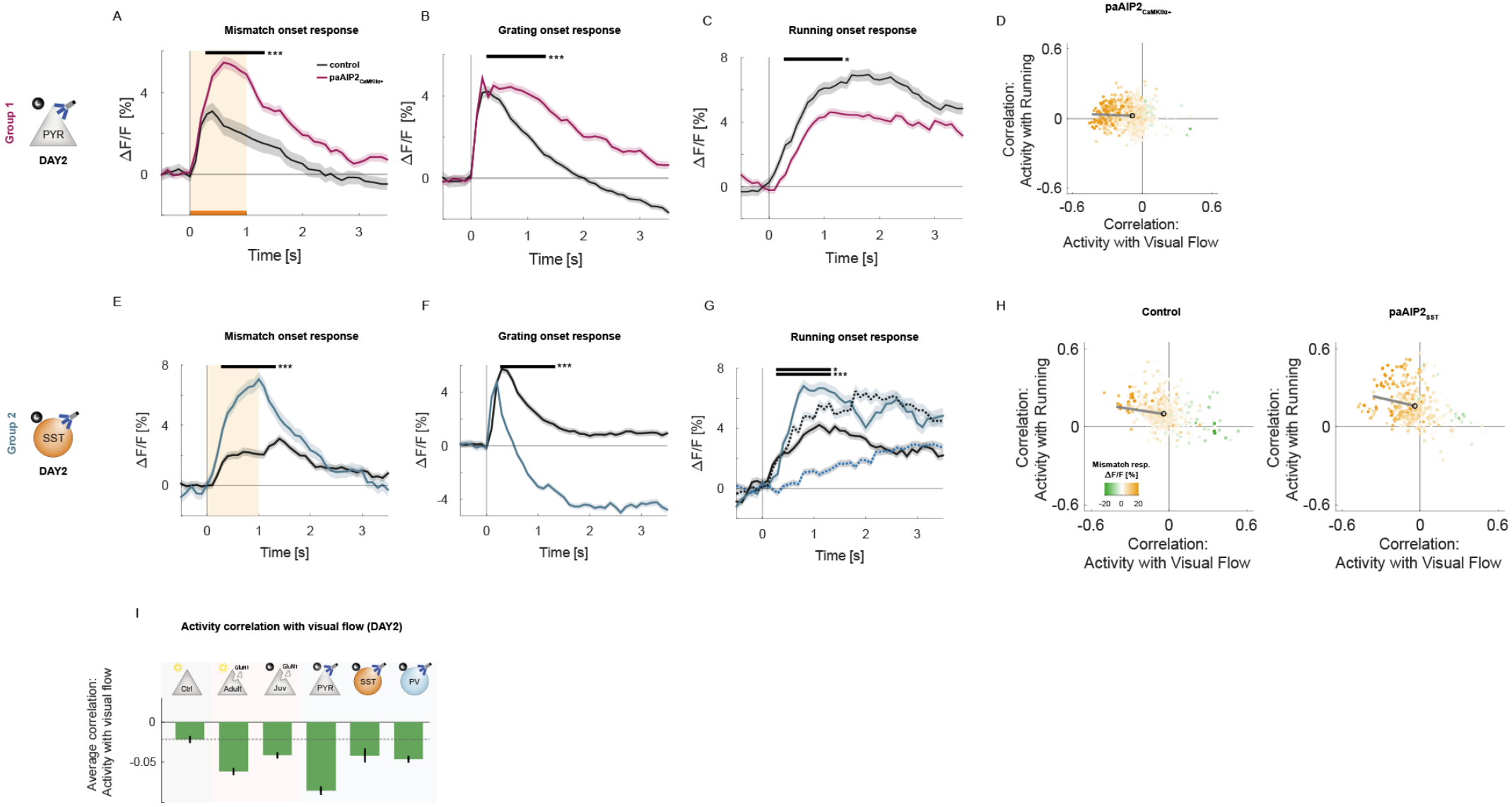
Group 1
PYR
DAY2
A
Mismatch onset response
control
paAIP2CaMKIIα
***
ΔF/F [%]
Time [s]
B
Grating onset response
***
ΔF/F [%]
Time [s]
C
Running onset response
*
ΔF/F [%]
Time [s]
D
paAIP2CaMKIIα
Correlation: Activity with Running
Correlation: Activity with Visual Flow
Group 2
SST
DAY2
E
Mismatch onset response
***
ΔF/F [%]
Time [s]
F
Grating onset response
***
ΔF/F [%]
Time [s]
G
Running onset response
*
***
ΔF/F [%]
Time [s]
H
Control
paAIP2SST
Correlation: Activity with Running
Correlation: Activity with Visual Flow
Mismatch resp. ΔF/F [%]
-20 0 20
I
Activity correlation with visual flow (DAY2)
Average correlation: Activity with visual flow
Ctrl
GluN1
Adult
GluN1
Juv
PYR
SST
PV

Figure S3. Changes by paAIP2 invert or revert over one day. Relates to Figure 5.

(**A**) The average population response (ΔF/F) to mismatch on day 2 of imaging was stronger in in paAIP2$_{CaMKII\alpha+}$ (purple) than in control (black) hemispheres. Orange area and bar indicate duration of mismatch; shading indicates SEM. The mean response of every neuron in the indicated horizontal bar (top) is compared using the rank-sum test, with the following denotation for significance. *p < 0.05, **p < 0.01 ***p < 0.001.

(**B**) Same as (**A**) but for moving grating responses following a grey screen.

(**C**) Same as (**A**) but running onset in closed-loop sessions.

(**D**) Correlation coefficients on day 2 of imaging between neural activity (ΔF/F) of layer 2/3 neurons with running speed and with visual flow in paAIP2$_{CaMKII\alpha+}$ hemisphere during open-loop sessions. Each dot represents a single neuron. Dot color indicates the amplitude of the mismatch response (ΔF/F [%]). Black circles indicate the mean correlation values. The solid black line indicates the angle between the first principle principal component of the distribution and the y-axis (see Methods).

(**E**) Same as (**A**) but for inhibition of paAIP2$_{SST}$ group on day 2 of imaging (inhibition in SST neurons, imaging in EF1α positive neurons).

(**F**) Same as (**E**) but running onset in closed-loop sessions.

(**G**) Same as (**E**), but for control and paAIP2$_{SST}$ hemispheres. Solid: Running onset responses in closed-loop sessions. Dotted: Running onset responses in dark sessions.

(**H**) Correlation coefficients between neural activity (ΔF/F) of layer 2/3 neurons with running speed and with visual flow in control (left) and paAIP2$_{SST}$ (right) hemisphere during open-loop sessions. Each dot represents a single neuron. Dot color indicates the amplitude of the mismatch response (ΔF/F [%]). Black circles indicate the mean correlation values. The solid black line indicates the angle between the first principal component of the distribution and the y-axis (see Methods).

(**I**) Mean correlation coefficients between neural activity (ΔF/F) of layer 2/3 neurons with visual flow in adult control animals and *ΔGrin1*$_{adult}$, *ΔGrin1*$_{juv}$, paAIP2$_{CaMKII\alpha}$, paAIP2$_{SST}$ and paAIP2$_{PV}$ knockout, resp. paAIP2 hemisphere.

METHODS

Animals and surgery

All animal procedures were approved by and carried out in accordance with Swiss guidelines of Canton Basel Stadt's Veterinary Department guidelines. For two-photon and behavioral experiments, mice were anesthetized with a standardized solution of Fentanyl (0.05 mg/kg; Actavis), Midazolam (5.0 mg/kg; Dormicum, Roche) and Medetomidine (0.5 mg/kg; Domitor, Orion). Analgesics were applied perioperatively (2% Lidocaine gel, Bichsel AG, Meloxicam 5mg/kg; Metacam, Boehringer Ingelheim) and post-operatively (Buprenorphine 0.1g/kg, Reckitt Benckiser Healthcare Ltd.). Eyes were carefully covered with ophthalmic gel (Virbac Schweiz AG). At postnatal day P21, we injected ca. 100nl of AAV2/1-Ef1α-Cre-T2A-mCherry, AAV2/1-EF1α-Cre-WPRE (**Figures 1-4**); AAV2/1-CaMKIIα(1.3kb)-mEGFP-P2A-paAIP2 or AAV2/1-EF1α-DIO-mEGFP-P2A-paAIP2-WPRE (**Figure 5**) through a small burr-hole on the right hemisphere at 2.25±.1mm lateral of lambda.

For dual window implantations at P30, we performed a standardized cranial window surgery of 4mm diameter (described in detail here: (Leinweber et al., 2014; Zmarz and Keller, 2016)) bilaterally, following injections of ca. 200nl of AAV virus (AAV2/1-EF1α-GCaMP6f-WPRE or AAV2/1-EF1α-NES-jRGECO1a-WPRE) into the target area primary visual cortex (V1), centered 2.5±.3mm AP/ML from lambda. All mice used had the same genetic background (C57BL/6) and were of the following genotype:

Mouse strain	**Source**	**Identifier**
B6.129S4-*Grin1*tm2Stl/J	from Jackson laboratories (JAX)	005246
C57BL/6J	from Charles River	-
PV-Cre	from JAX	008069
SST-Cre	from JAX	018973

These are the AAV constructs that were used:

Vector	**Source**	**Identifier**
AAV2/1-EF1α-GCaMP6f-WPRE	FMI vector core (vector.fmi.ch)	-
AAV2/1-EF1α-Cre-t2a-mcherry-WPRE	FMI vector core	-
AAV2/1-EF1α-Cre-WPRE	FMI vector core	-
AAV2/1-EF1α-NES-jRGECO1a-WPRE	FMI vector core	-
AAV2/1-CaMKIIα(1.3kb)-mEGFP-P2A-paAIP2	Addgene	91718
AAV2/1-EF1α-DIO-mEGFP-P2A-paAIP2-WPRE	FMI vector core	-

Virtual reality and skill learning task

During all experiments involving the virtual reality setup, mice were head-fixed and mounted on a polystyrene ball as described previously (Leinweber et al., 2014). In brief, mice were free to run on a polystyrene, spherical ball. Mice were restricted to run only in one dimension for two-photon imaging experiments (forwards or backwards).

For behavioral experiments, animals were free to turn clockwise or counter-clockwise, in addition to running forwards and backwards. The tunnel expansion was automated and restricted to positive expansion only. The tunnel expanded every 4 rewards by a ratio between 20 seconds and time spent until reward, to a maximum of 1.5, starting with a minimum of 25 virtual units (VU), to a maximum of 100 VU at full tunnel length.

For the skill learning, task performance index was calculated as follows:

$$Performance = \frac{\cos(\theta) * distance_{traveled}}{total\ distance} * \frac{time\ spent\ running}{total\ time}$$

Where θ is the angle ranging from representing ±180° to left (or right) in the virtual reality. The performance index was defined as distance traveled towards the target divided by total distance travelled, multiplied by the fraction of time spent running. Using this measure, either a random walk, or no movement results in a performance of 0, where continuous movement in a straight line towards the target results in a performance of 1.

Two-photon calcium imaging

All data was recorded as described in detail previously (Leinweber et al., 2014, 2017)). In brief, all two-photon imaging data was recorded using a modified Thorlabs Bergamo I or II microscope. Excitation light was emitted by a tunable, femtosecond-pulsed laser (Insight, Spectra Physics, used at 910 or 980nm for GCaMP6f, 1030nm for jRGECO1a), directed with a XY galvanometer system (based on 8 or 12 kHz resonant scanner, Cambridge Technology) and split into 4 z-layers using a piezo electric linear actuator (P-726, Physik Instrumente) and passed through a 16x, 0.8 NA objective (Nikon). Emission light was band-pass filtered using a 525/50 or a 607/70 filter (Semrock), detected by a photomultiplier tube (PMT, H7422P, Hamamatsu), amplified (DHPCA-100, Femto), digitized at 800 MHz (NI5772, National Instruments) and band-pass filtered at 80 MHz by digital Fourier transform on a field-programmable gate array (FPGA, NI5772, National Instruments, loaded with custom-designed logic). Images were acquired and written to disk at 750 x 400 px using LabView (software available on the public GitHub repository, see materials), with 10 or 15 frames per z-plane and a field of view of approx. 375 µm x 300 µm.

If possible, all animals were imaged on both hemispheres. Some animals (for precise list see **Table 1**) could only be imaged on one hemisphere because the imaging quality did not meet our minimal standards (<30-40mW total laser power, activity visible by eye in live view).

Unless otherwise noted, all two-photon imaging data was acquired in sessions of 5-10 minutes, in the following sequence: Closed-loop, open-loop, dark, grating. The visual stimuli were sinusoidal gratings and projected to toroidal screen surrounding the mouse (covering approx. 240 deg. horizontally and 100 deg. vertically of its visual field). During closed-loop, a tunnel of vertically arranged gratings were coupled to the mouse's locomotion speed. In open-loop sessions, the visual stimuli of the closed-loop session were replayed. In grating sessions, a gray screen followed by a pseud-randomly chosen moving-grating stimuli, one of eight (0, 45, 90, 270 deg. moving in either direction), were presented with randomized onset time of 3-6s.

Conditional *Grin1* knockout and Histology

All *ΔGrin1* knockout experiments were performed using fNR1 featuring a conditional knockout of *Grin1*, coding for GluN1, a subunit described to be essential to the NMDA receptor (Monyer et al., 1994). We confirmed the knockout using mRNA in-situ hybridization (RNAscope, Ventana) in separate animals from the parents, 14 days post injection for both datasets ($\Delta Grin1_{juv,\ adult}$). We followed a standardized FFPE (Formaldehyde-fixed paraffin-embedded), in brief: After brain harvesting, storage in 4% PFA overnight (standard temperature and humidity), paraffinization over 24h, 5µm microtome (ThermoFisher) slices and staining using hematoxylin for cell bodies and the Mm-*Grin1*-O1 (#473079, target region 2892 - 4127, ACDBio) to stain *Grin1* mRNA (full Ventana protocol available on request). For most experiments a vector co-expressing a red fluorophore (mCherry) was used for easy identification of the knockout area in two-photon microscopy. As the injection site in adult animals ($\Delta Grin1_{adult}$) did not change over time as was the case for juvenile animals ($\Delta Grin1_{juv}$), we omitted the red fluorophore in some animals ($\Delta Grin1_{adult}$ dataset, 7/14 animals).

Optogenetic activation of paAIP2

To inhibit Calcium/calmodulin-dependent kinase II (CaMKII) using a photoactivatable autocamtide inhibitory peptide 2 (paAIP2) during visuomotor exposure in the virtual reality environment, we followed the protocol of original publication (Murakoshi et al., 2017). As illumination source of blue light, we used a laser (OBIS 473nm LX 75mW, Coherent), a galvo-galvo system and a set of mirrors and lenses (GVSM002-EC/M, Thorlabs) to redirect the beam onto the brain surface (2.5-3cm diameter, centered on V1). We followed the duty-cycle outlined by (Murakoshi et al., 2017) of 1s on and 4s off. During the 1s on time, we redirected the laser to illuminate both hemispheres equally (switching hemispheres every 20ms). The time-averaged total laser power was 2mW/s with an estimated average illumination area of 6±1.1mm^2.

Extraction of neuronal activity and data analysis.

Calcium imaging data was processed as described previously (Keller et al., 2012). In brief, raw images were full-frame registered to correct for brain motion. Neurons were selected manually (based on mean and maximum fluorescence images). Average fluorescence per selected region over time was corrected for slow fluorescence drift using an 8th percentile filtering (Dombeck et al., 2007) and divided by their median.

Data analysis was performed with custom analysis scripts in MATLAB 2020b (MathWorks). For all population onset responses, data was averaged over onsets and concatenated over neurons. Unless otherwise stated, shading or error bars indicates the standard error of the mean (SEM) over the average neuron response to a given event of interest. Because sites with particularly few onset responses (less than 3) tended to dominate the average response, we excluded this data in all plots shown. The baseline subtraction window was -300ms to 0ms, the window for calculating significance was +300ms to +1300ms after onset. Unless stated otherwise in figure legends, the significance test consisted of two-sided rank-sum test with default parameters. The running threshold was ca. 10^{-2} cm/s. We calculated Pearson's correlation coefficient between neural activity and visual flow or running speed during the open-loop sessions.

Imaging summary

We imaged all experimental animals on both hemispheres whenever possible, with the left hemisphere being the control hemisphere, and the right the experimental one. The table below lists all datasets, how many animals were included, and how many were imaged on both or the respective hemisphere. Percentages rounded to two decimal places.

Table 1

	Imaged hemispheres				Total number of ROIs		
Dataset	Left only	Right only	Both	Total	Left	Right	Total
Δ*Grin1*$_{juv}$	4	5	10	19	2625	1986	4611
Δ*Grin1*$_{adult}$	1	3	10	14	1281	1547	2828
paAIP2$_{CaMKIIα}$	0	0	6	6	781	928	1709
paAIP2$_{SST}$	1	0	5	6	1149	872	2021
paAIP2$_{PV}$	0	0	6	6	1575	1120	2695

Data and code availability

Requests for data and software should be directed to and will be fulfilled by the Lead Contact, Georg B. Keller (georg.keller@fmi.ch).

Resource	**Availability**
Software for microscope control	sourceforge.net/projects/iris-scanning
Software for processing calcium imaging data	sourceforge.net/projects/iris-scanning
Information about vectors from FMI vector core:	vector.fmi.ch
Data to generate the figures of this chapter:	data.fmi.ch

Acknowledgements

We thank all the members of the Keller lab for discussion and support, and Tingjia Lu and Danila Gerosa for the virus production**.** This project has received funding from the Swiss National Science Foundation (GBK), the Novartis Research Foundation (GBK), and the European Research Council (ERC) under the European Union's Horizon 2020 research and innovation programme (grant agreement No 865617) (GBK).

Author contributions

FW designed and performed the experiments and analyzed the data. All authors wrote the manuscript.

Declaration of Interests

The authors declare no competing financial interests.

CHAPTER II: EFFECTS OF ANTIPSYCHOTICS

Abstract. Psychosis summarily describes a clinical phenotype, composed of symptoms like delusions and hallucinations. Antipsychotic drugs effectively ameliorate many of these symptoms, despite differences in their diverse receptor binding profiles. Here, we probed whether applying three clinically effective antipsychotic drugs (Haloperidol, Clozapine and Aripiprazole) show a functional signature in neuronal activity of mouse primary visual cortex (V1). One of the most common changes was a decrease in visuomotor prediction errors in layer 2/3 neurons. Clozapine, as one of the clinically most effective drugs, likely decreased activity of inhibitory neurons thought to mediate visual feedforward signals and increased the mean activity in layer 5. However, we did not find common changes to all three antipsychotic drugs we investigated. Previous research with pharmacological models reproduced symptoms of psychosis and found reduced responses to visual stimuli in V1. We find that antipsychotic drugs did not increase visual responses, instead more likely act by affecting how visual and motor-related responses are integrated.

INTRODUCTION

A brief history of antipsychotics. In 1949, the French army surgeon Henri-Marie Laborit explored anesthetic substances and discovered a calming cocktail (a group of phenothiazine derivatives) that he used as an anxiolytic, and to lessen post-surgery 'shock'. The research on phenothiazines continued until a chlorinated derivative of promazine was found, eventually named chlorpromazine. Early studies observed a group of symptoms associated with decreased motor activity and affective indifference, which was named 'neuroleptic syndrome', translating loosely to 'to take the nerve off'. Using this drug, psychiatric patients became more manageable, decreasing hospital beds used for schizophrenia, and clinicians noted reduced excitement in acutely psychotic patients. Some patients even appeared as if they had recovered, and this paved the way for a 'neuro-biological' basis of psychiatric diseases (López-Muñoz et al., 2005).

Chlorpromazine was, however, not efficacious in apathetic and deteriorated patients. Further, it showed extrapyramidal side effects (EPS), commonly referred to as drug-induced movement disorder from dopamine-receptor blocking agents (D'Souza and Hooten, 2021). The term 'neuroleptic' for chlorpromazine and subsequently dopamine antagonist drugs captured both the tranquilization and neurological effects. The term 'antipsychotic' was then used to delineate the behavioral effects of chlorpromazine as compared to other, more sedative drugs ('tranquilizers'), which proved ineffective in schizophrenia patients.

Multiple drugs following Chlorpromazine were developed, including Haloperidol. Haloperidol, a butyrophenone derivative, was synthesized in 1958 at a Belgian laboratory by Paul Janssen while trying to develop a more powerful analgesic. Haloperidol was not more effective than morphine, however it was found to sedate mice which went into a cataleptic state, similar to that produced by chlorpromazine. Haloperidol was (and still is) effective against delusions and hallucinations (known as 'positive symptoms' in schizophrenia). Unfortunately, Haloperidol also showed EPS, similar to chlorpromazine; both of these drugs were also ineffective in apathetic or anhedonic patients (known as 'negative symptoms' in schizophrenia) and more compounds were developed (with comparable efficacy, thought to mainly act through dopamine antagonism).

Additionally, in 1958, compounds based on the antidepressant imipramine were developed, with neuroleptic properties, Clozapine standing out as one that did not cause cataplexy in animal studies. Studies comparing Clozapine with Chlorpromazine followed, showing effectiveness without strong EPS side effects, and interestingly, seemed to be effective also in patients with negative symptoms. Because efficacy of antipsychotic drugs up until then were associated strongly with EPS, the terms 'typical' and 'atypical' antipsychotic were introduced, with the former being more prone to EPS side-effects. (Carpenter and Davis, 2012; Ramachandraiah et al., 2009).

Today, Clozapine still is one of the most effective antipsychotics drugs (Huhn et al., 2019) even if several barriers surrounding the administration, management, and monitoring by clinicians and adherence by patients. Therefore other drugs like Aripiprazole are recommended as first-line antipsychotic treatment (Farooq et al., 2019; Tungaraza and Farooq, 2015). All of the current antipsychotic drugs are still not highly effective and have several (and severe) side effects, which has become a major point for deciding first-line therapy. Given that little to no progress has been made (in terms of creating better antipsychotic alternatives) it is clear that we need a new way to approach the problem.

Antipsychotic drug research. Based on receptor affinities and measured clinical efficacy, several hypotheses have been generated about the mechanism of action in antipsychotic drugs, however there is no consensus as to which receptors are the most important (Nucifora et al., 2017). Clinically, antipsychotics are still categorized into typical and atypical antipsychotics, referring to the sedative action of the first antipsychotic agents; however, this classification may be historical and not based on receptor binding profiles or molecular targets (Leucht et al., 2009).

To develop new drugs and predict outcomes, several animal assays have been used for pre-clinical testing; here, the approach so far was to revert mimicked symptoms of psychiatric diseases. Besides genetic models using knockouts (e.g., DISC-1, Dysbindin), there are pharmacological models that are

typically more accessible, such as PCP (also known as 'angel dust'; an NMDA receptor antagonist) or high doses of Amphetamine (which can cause psychotic states in humans (Bramness et al., 2012)). However, Amphetamine models fail to reproduce negative symptoms and, most of the time, are investigated in adult animals. Amphetamine has therefore been criticized in that it does not capture the developmental aspects of psychiatric diseases. A review on animal models in schizophrenia attributes failure to develop new therapeutics to the lack of understanding of the underlying disease mechanisms. Adding to this, animal models of psychiatric diseases (especially schizophrenia) have shown low predictive power, with a tendency to overstate actual clinical efficacy (Jones et al., 2011).

A better understanding of psychiatric disease pathophysiology and a better understanding of isolated symptoms could improve predictive power of animal models. One way to study symptoms is to investigate how hallucinogens achieve their effect, and this is currently actively researched. Especially notable is the agonistic action on the Serotonin receptor 2A (5-HT_{2A}R), causing visual hallucinations in humans that are ameliorated with 5-HT_{2A}R inhibitors (Vollenweider et al., 1998). Interestingly, serotonin 2A agonists also cause behavioral changes in mice,(and are notably absent in 5-HT_{2A}R knockout mice (Halberstadt et al., 2009). Unfortunately, in many countries, research on these drugs is hampered because of historical stigma and consequent regulations, greatly restrict research.

To summarize, psychiatric diseases are largely classified and treated symptomatically. Serendipitously, effective drugs were discovered, and some of the early drugs that were discovered remain the most effective, even to this date. Investigating drugs that reliably reproduce specific symptoms, like hallucinations, have been hindered by regulations. Animal models using genetic or pharmacological approaches have a lot of potential to improve their accuracy in terms of predicting clinical efficacy of new compounds. Why different receptor binding profiles lead to different clinical outcomes is still unclear. One approach to investigate how antipsychotic agents achieve efficacy, is to examine how they function at the level of neuronal circuitry. Importantly, if there were a core set of circuit correlates which could help define a successful antipsychotic, it could improve and speed up the development of treatment alternatives, which was the motivation for the work presented in this chapter.

Experimental approach. Using the experimental approach from **Chapter I**, a virtual environment in combination with *in-vivo* two-photon calcium imaging, we can identify neuronal responses in layer 2/3 of mouse primary visual cortex, and a recent review summarizes a circuit working-model (Keller and Mrsic-Flogel, 2018). Using this information and approach, we speculated to find a functional signature of antipsychotic drugs: a set of common changes in e.g., motor-related, visual or visuomotor mismatch responses.

Such an idea would also be in line with the literature, given that in psychosis the balance between predictions and sensory data has been proposed to be disrupted, leading to faulty prediction errors (Fletcher and Frith, 2009). It is not exactly clear how this imbalance arises at a neurobiological level, but multiple authors suggest that prediction error signals are affected (Sterzer et al., 2018). Given that antipsychotic agents can ameliorate symptoms in psychiatric diseases (Leucht et al., 2017), they are speculated to work in an opposing fashion to the computational (and/or structural) changes associated with the pathological state. Regardless, prediction error signals should serve as a common intersection point between different antipsychotics (different referring to the highly varied and sometimes antagonistic receptor binding profiles of these drugs) but proven antipsychotic chemicals.

To this end, we systemically injected three antipsychotic agents (identified as effective under clinical contexts (Huhn et al., 2019)), to achieve two aims: 1) To characterize the changes associated with antipsychotic agents in a primary sensory area at the neuronal level, and 2) to probe for a convergent set of changes at a functional level, that may help probe the efficacy of future antipsychotic compounds (functional signature). We found no single functional signature common to all three drugs. Most commonly we observed a decrease in the negative prediction error response to visuomotor mismatch (visual-flow halts during closed-loop condition). While this change was absent in Haloperidol, Haloperidol decreased activity correlation with visual flow. Additionally, we examined Clozapine more closely and found that it induced a decrease in SST neuron activity and an increase in layer 5 pyramidal cell activity. Within the predictive processing framework, these changes could be consistent with the interpretation of reduced bottom-up input integration, resulting in lower prediction error signals and an increase in persistent activity of representational units.

RESULTS

To probe for a set of common functional signatures of different antipsychotic drugs, we injected three different antipsychotic substances (Haloperidol, HAL; 0.1mg/kg, Clozapine, CLO; 0.1mg/kg and Aripiprazole, ARI; 0.1mg/kg) or saline (SAL) in separate cohorts of mice. We measured visual, motor-related and visuomotor mismatch responses in primary visual cortex 24h before (abbreviated 'pre') and 24h after (abbreviated 'post') injection (**Figure 1, A1-3)**. As many antipsychotics, especially Haloperidol, show a suppressive effect on locomotion, we chose a dose where animals still would run (see Methods).

Because visuomotor mismatch responses in primary visual cortex are likely computed by integration of both sensory and locomotion-related signals (Attinger et al., 2017; Keller and Mrsic-Flogel, 2018; Leinweber et al., 2017; Zmarz and Keller, 2016), these responses were the focus of our primary analysis. Comparing the population response of the same neurons pre and post drug application to mismatch, we found that responses were reduced in CLO and ARI (**Figure 1, B3-4**), while HAL and saline groups did not show a reduction (**Figure 1, B1-2**). We also measured population responses to running and drifting gratings. We found an increased running-onset response post CLO and a decreased (or delayed) response post ARI (**Figure 1, C1-4**), and again HAL did not induce a change in response. Visual responses were consistently lower post SAL and all three types of antipsychotic injections (**Figure 1, D1-4**). The fact that grating responses are reduced post SAL indicates a physiological reduction of grating response over multiple presentations. This adaptation may partially or completely account for the reduction in visual signals post antipsychotic injection.

To assess where the reduction in mean population mismatch response comes from, we split the data into the top 10% and least 10% responsive neurons to mismatch and found that the most responsive neurons drove the effect for CLO and ARI, whereas the least responsive neurons showed no significant difference (**Figure S1, A1,3**). The overall fraction of neurons that respond with increase in calcium during mismatch showed a mild (and non-significant) decrease post antipsychotic injection (**Figure S2, A2-4**), whereas saline controls had an opposite trend (**Figure S2, A1**).

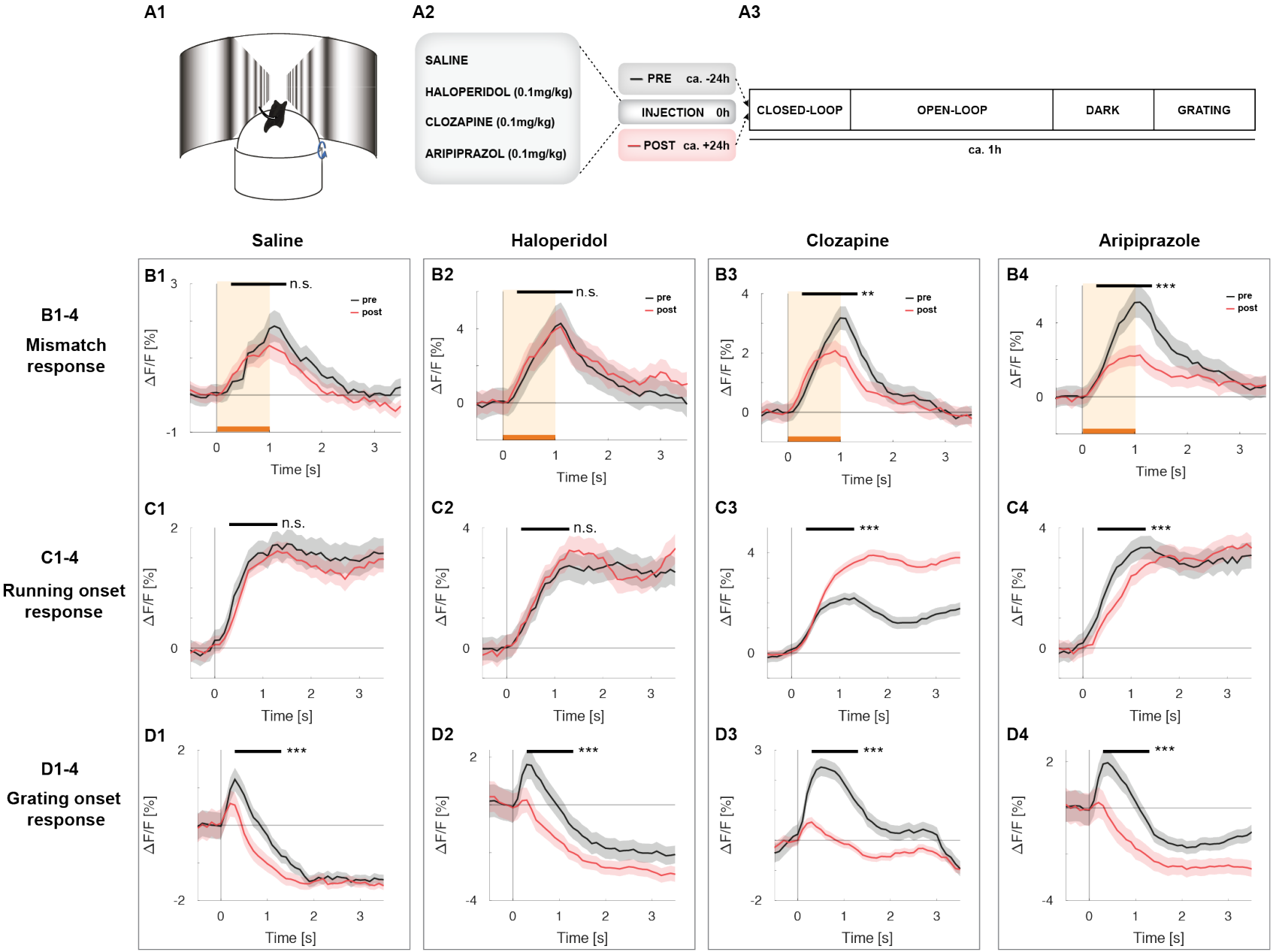
A1
A2
A3
SALINE
HALOPERIDOL (0.1mg/kg)
CLOZAPINE (0.1mg/kg)
ARIPIPRAZOL (0.1mg/kg)
PRE ca. -24h
INJECTION 0h
POST ca. +24h
CLOSED-LOOP
OPEN-LOOP
DARK
GRATING
ca. 1h
Saline
Haloperidol
Clozapine
Aripiprazole
B1-4
Mismatch response
C1-4
Running onset response
D1-4
Grating onset response
B1
B2
B3
B4
C1
C2
C3
C4
D1
D2
D3
D4
n.s.
**
***
pre
post
ΔF/F [%]
Time [s]

Figure 1. Characterization of visual, running and mismatch responses.

(**A**) Experimental setup and paradigm. A1: Schematic of virtual reality tunnel. Mice were restricted to movement in one dimension. A2: Injected drugs and dosages. A3: Experimental timeline. Both pre (ca 24h prior drug injection) and post (ca. 24h post drug injection) timepoints followed the same experimental procedure, starting with a closed-loop session (visual flow is coupled to the mouse's locomotion speed), followed by 2-3 open-loop sessions, where visual flow from closed-loop was replayed. During dark, the virtual reality setup was off and all lights in the room covered. During grating, a sequence of gratings was presented following a grey screen.

(**B**) B1: Mismatch response (ΔF/F [%]) pre (black) and post (red) saline injection, averaged over trials and neurons, error bar shading indicates SEM over neurons. Orange shading and horizontal bar indicate onset and duration of visual flow halt. Significance was tested using rank-sum for the black, horizontal bar (top). Legend: *p<0.05, **p<0.01, ***p<0.001. B2-4: Same, but for Haloperidol, Clozapine and Aripiprazole.

(**C**) C1-4: same as (**B**) but for running onset response.

(**D**) D1-4: same as (**B**) but for grating onset response. These responses are averaged over all trials and included grating onsets during moving and stationary periods.

Neurons activated by mismatch (MM+, see Methods) typically exhibit a specific type of activity correlation reflective of their visuomotor integration profiles (Attinger et al., 2017): A positive correlation of activity with running and a negative correlation with visual flow (P-V). Interestingly, we found that while the mismatch response amplitude tended to be reduced in MM+ neurons post antipsychotic injection, the fraction of neurons consistent with coding a visuomotor prediction error (here, operationally defined as 'expected correlation') had a propensity to increase slightly (but non-significantly) post HAL and ARI, and CLO (**Figure 2, A2-4**), with an opposing trend post saline (**Figure 2, A1**). This trend was also opposed in preliminary data of a low-dose pro-psychotic agent A (see Methods) we tested in a pilot study (**Figure S3, E1-2)**. The same trend continued to be true for other, higher thresholds, above zero (**Figure S2, B1-4**). Generally, MM+ neurons exhibited the expected correlation and other neurons show a positive correlation with both visual flow and running pre and post drug injection (**Figure 2,** c.f. pre **B1-4** and post **C1-4**).

Interestingly, post antipsychotic injection, more neurons in the MM+ fraction clustered in the upper-left quadrant for different reasons: post SAL, the reduced fraction can be explained with a net increase in visual and running correlation. Post HAL, the fraction is increased because of a net decrease of visual correlation and post CLO, the increase can be explained by an increase in running correlation (**Figure 2, D1-2**). Neurons post ARI show the same trends as post SAL, which may seem contradictory given the trend of MM+ post ARI not to change their correlation sign on average unlike SAL with the opposite trend (**Figure 2,** c.f. **A1** and **A4**). This could be explained by MM+ post ARI reducing their correlation maxima while maintaining the position in the upper-left quadrant, unlike MM+ post SAL (**Figure 2,** c.f. **B1, C4** and **B4, C4**).

Overall, however, there was no common change in activity correlation with visual flow and running post antipsychotic injections (**Figure 2, D1-2**). We further quantified the linear change per-neuron, rather than overall mean-shift. Interestingly, we observed a remarkably similar amount of linear change post SAL and post antipsychotic injection (**Figure S2, C1-4**) with correlation coefficients between 0.61 to 0.65, even for HAL. This is contrasted by correlation with running, where there was a more common trend of a reduction in correlation coefficient, with a reduction for neurons pre/post CLO (**Figure S2, D1-4**). The non-linear change post antipsychotic injection could be due to a selective change of activity correlation in different genetic or functional neuronal subpopulations; we probed for highly running-onset, mismatch onset or grating onset responsive neurons, however we did not find any significant deviation from the population correlation for these groups (data not shown).

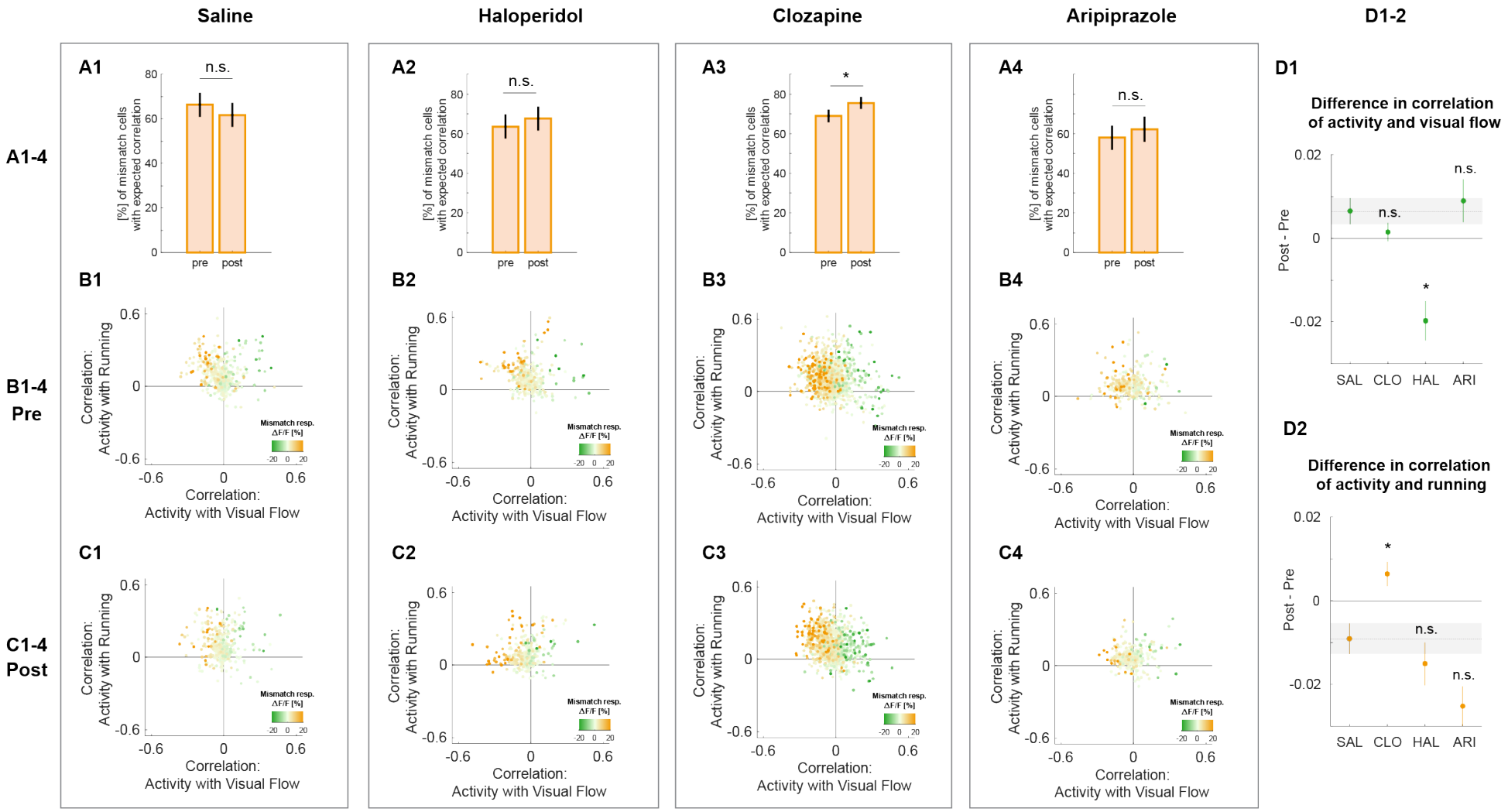
Saline
Haloperidol
Clozapine
Aripiprazole
D1-2
A1-4
B1-4
Pre
C1-4
Post
A1
A2
A3
A4
n.s.
*
[%] of mismatch cells with expected correlation
pre
post
B1
B2
B3
B4
C1
C2
C3
C4
Correlation: Activity with Running
Correlation: Activity with Visual Flow
Mismatch resp. ΔF/F [%]
D1
Difference in correlation of activity and visual flow
Post - Pre
SAL
CLO
HAL
ARI
D2
Difference in correlation of activity and running

Figure 2. Correlational analysis during open-loop.

(**A**) **A1**: Fraction of neurons [%] with positive activity correlation to running and negative to visual flow of all neurons that showed an increased calcium response to mismatch onsets on average. Numbers on top of the bars indicate the absolute number of neurons with positive mismatch response. Error bars indicate 95% confidence interval obtained by bootstrap (10'000 repeats, with replacement). * indicates confidence intervals do not overlap (n.s. indicates they overlap). **A2-4**: same as A1, but post Haloperidol, Clozapine and Aripiprazole.

(**B**) Correlation coefficient of every neuron's activity with visual flow (X-axis) and with running (Y-axis) pre drug injection. Color indicates mean response to mismatch onset (in closed-loop) during significance window.

(**C**) same as (**B**) but post drug injection.

(**D**) **D1-2**: Difference in mean pre and post drug injection for correlational data in (**B1-4, D1**) and (**C1-4**, **D2**). Every neuron's mean correlation was subtracted (post-pre). Error bars indicate SEM over neurons (after subtraction). *p<0.05, n.s.: p>=0.05, Kruskal-Wallis test.

Previous research showed that neurons activated by mismatch are likely disinhibited during a mismatch event by somatostatin positive (SST) neurons, a well-characterized subpopulation of inhibitory neurons in primary visual cortex, highly responsive to visual stimuli. We therefore tested whether the clinically most-effective antipsychotic, CLO, would modulate SST activity, with four possible outcomes: a) SST neurons are tonically more a_1) activated or a_2) deactivated or b) SST neurons show a change in gain, either b_1) increased or b_2) decreased – or any combination thereof. Any of these possibilities alone would lead to a decrease of mismatch response (**Figure S3, D2**). The combination of a_1 and b_1 could lead to an increase in mismatch response. We found that SST neurons post CLO have a reduced amplitude in the response to mismatch (**Figure 3, A1**) and the population trended to decrease in overall activity (approx. -37% ΔF/F, p=0.47, rank-sum test, **Figure 3, A2**). Because there were significant differences in running behavior (data not shown), we speed-matched the mismatch response (see methods); this increased the effect size indicating the effect is independent of differences in running speed (**Figure S3**, **A1**). During two-photon imaging over multiple days, we would expect mean raw fluorescence to slightly increase over time because of increased viral expression. Given that we used consistently the same technical parameters to record the data, we also compared absolute fluorescence and found a decrease of 14% ($p<0.001$, rank-sum test) consistent with the previously characterized trend (**Figure 3, A3**). These findings are consistent with a decrease in SST activity post CLO. SST neurons post CLO showed an increase in mean visual correlation and a high correlation coefficient (**Figure S3, A2;** $r_{Pearson} = 0.77$), whereas the mean correlation with running decreased, and showed a low correlation coefficient (**Figure S3, A3;** $r_{Pearson} = 0.33$), indicating SST neurons were de-correlated with running post CLO. We did not have a direct control for these animals but re-analyzing data from previous experiments ((Attinger et al., 2017), coupled-trained animal group), we found there is a (smaller) trend of reduced overall activity (-11%, p=0.72, rank-sum test, **Figure S3, C2**), with no change in mismatch response over two days (**Figure S3, C1**).

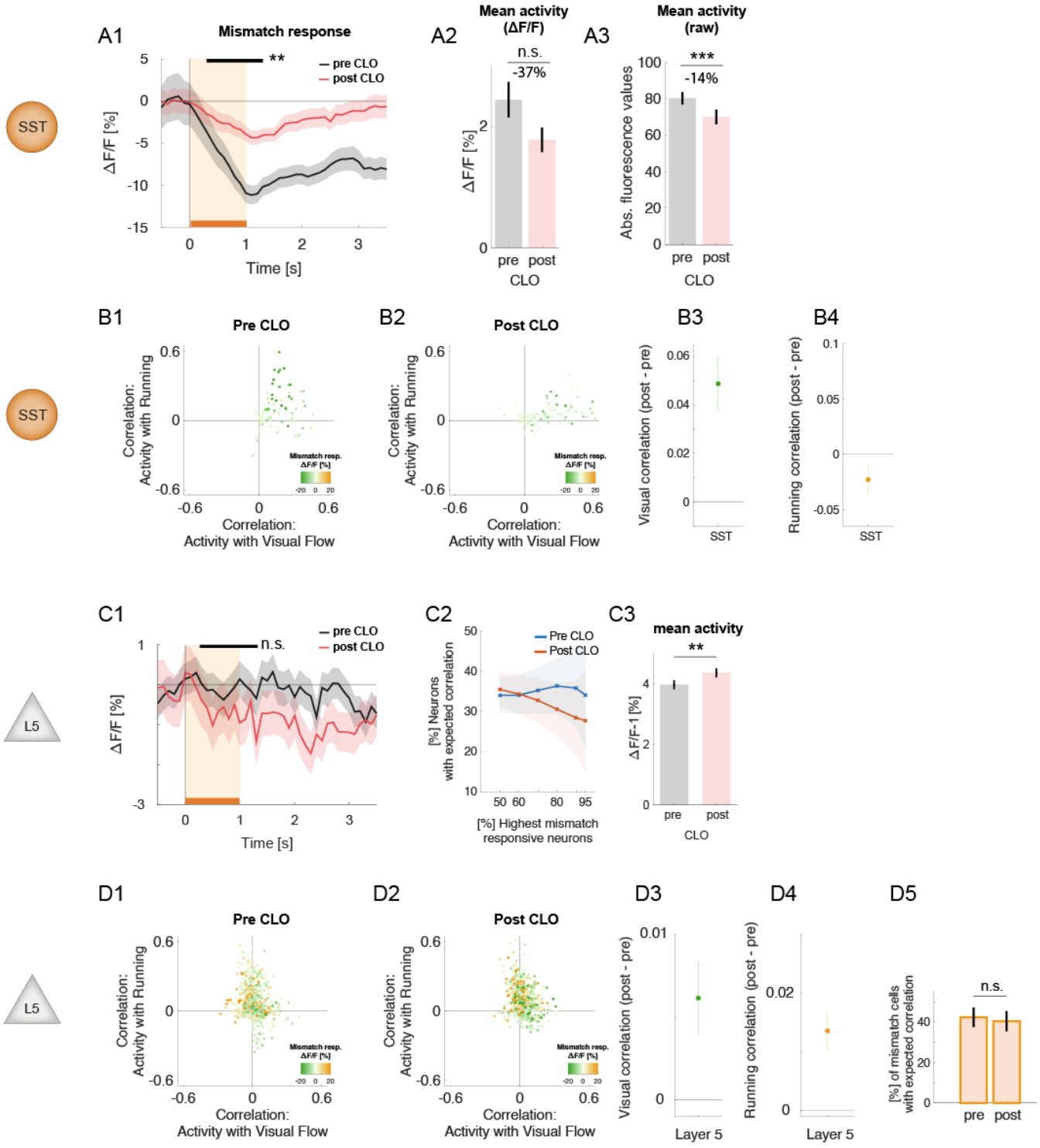
SST
A1
Mismatch response
**
pre CLO
post CLO
ΔF/F [%]
Time [s]
A2
Mean activity (ΔF/F)
n.s.
-37%
ΔF/F [%]
pre post
CLO
A3
Mean activity (raw)
***
-14%
Abs. fluorescence values
pre post
CLO
SST
B1
Pre CLO
Correlation: Activity with Running
Correlation: Activity with Visual Flow
Mismatch resp. ΔF/F [%]
B2
Post CLO
B3
Visual correlation (post - pre)
SST
B4
Running correlation (post - pre)
SST
L5
C1
n.s.
pre CLO
post CLO
ΔF/F [%]
Time [s]
C2
Pre CLO
Post CLO
[%] Neurons with expected correlation
[%] Highest mismatch responsive neurons
C3
mean activity
**
ΔF/F-1 [%]
pre post
CLO
L5
D1
Pre CLO
Correlation: Activity with Running
Correlation: Activity with Visual Flow
Mismatch resp. ΔF/F [%]
D2
Post CLO
D3
Visual correlation (post - pre)
Layer 5
D4
Running correlation (post - pre)
Layer 5
D5
n.s.
[%] of mismatch cells with expected correlation
pre post

Figure 3. Clozapine effects in SST neurons and layer 5.

(**A**) **A1**: Mismatch response (ΔF/F [%]) pre (black) and post (red) Clozapine injection, averaged over trials and neurons, error bar shading indicates SEM over neurons. Orange shading and horizontal bar indicate onset and duration of visual flow halt. Significance was tested using rank-sum for the black, horizontal bar (top). Legend: * p<0.05, **p<0.01, *** p<0.001.

A2: Mean activity (ΔF/F [%] - 1) pre and post Clozapine during the whole experiment. Error bars indicate SEM over neurons. Activity was not different (rank-sum test p=0.47), but tended towards reduction (-37.01%).

A3: Mean activity as measured from raw fluorescence during the whole experiment. Error bars indicate SEM over neurons. Activity was reduced (-14.61%, p<0.001, rank-sum test).

(**B**) B1: Correlation coefficient of every (SST) neuron's activity with visual flow (X-axis) and with running (Y-axis), pre Clozapine. Color bar indicates mean response to mismatch onset (in closed-loop) during significance window.

B2: Same as B1, but post Clozapine.

B3: Quantification of mean shift in correlation of activity with visual flow (post-pre) in B1.

B4: Quantification of mean shift in correlation of activity with running (post-pre) in B2.

(**C**) **C1**: Mismatch response (ΔF/F [%]) pre (black) and post (red) Clozapine injection in layer 5 neurons, averaged over trials and neurons, error bar shading indicates SEM over neurons. Orange shading and horizontal bar indicate onset and duration of visual flow halt. Significance was tested using rank-sum for the black, horizontal bar (top). Mismatch response was not different pre and post Clozapine in layer 5 (p=0.14, rank-sum test).

C2: Fraction of neurons [%] with positive activity correlation to running and negative to visual flow of all neurons (Y-axis) that showed an increased calcium response to mismatch onsets on average, as a function of increasing percentile cut-offs of highest-responding cells to mismatch (X-axis) pre (blue) and post (red) Clozapine.

C3: Difference in mean activity over the whole experiment, pre and post Clozapine in layer 5 neurons. Error bar indicates SEM over neurons. There was an increase in mean activity post Clozapine (p=0.0021, rank-sum test).

(**D**) D1: Correlation coefficient of every layer 5 neuron's activity with visual flow (X-axis) and with running (Y-axis), pre Clozapine. Color bar indicates mean response to mismatch onset (in closed-loop) during significance window.

D2: same as D1, but post Clozapine

D3-4: Quantification of mean shift (post-pre) from **D1-2**.

D5: Fraction of neurons [%] with positive activity correlation to running and negative to visual flow of all neurons that showed an increased calcium response to mismatch onsets on average. Numbers on top of the bars indicate the absolute number of neurons with positive mismatch response. Error bars indicate 95% confidence interval obtained by bootstrap (10'000 repeats, with replacement); n.s. indicates overlap of confidence intervals.

Finally, we investigated changes post CLO in layer 5 neurons. Here, the predictive processing framework (Keller and Mrsic-Flogel, 2018) predicts that signals consistent with internal representation are present in infragranular layers of cortex. If the model holds true, a decrease in negative prediction errors may therefore decrease the inhibitory activity in layer 5 of visual cortex. Consistent with this, we found an increase in mean activity in layer 5 post CLO. Further consistent with the model in general, we found less neurons correlated with running and anticorrelated with visual flow pre and post CLO (**Figure 3, D1-2**). Further, post CLO there was a trend towards an increase in correlation of layer 5 activity with running and with visual flow (**Figure 3, D3-4**), with similar linear relationships pre and post CLO for visual and running correlation (**Figure S3, C2-3;** visual flow $r_{Pearson}$=0.58, running $r_{Pearson}$=0.62).

DISCUSSION

We characterized motor-related, visual and visuomotor mismatch signals in primary visual cortex of mice, pre and post antipsychotic drug (or saline) injection. We found that visual responses were decreased in all animals (including controls); running-related responses and visuomotor mismatch responses were changed post atypical (Clozapine, Aripiprazole), but not typical antipsychotic (Haloperidol) drug administration.

We probed for a functional signature, a common set of changes among the three investigated agents at network level and have not found significant differences common to all drugs. There were, however, common changes and trends: All antipsychotic drugs decreased responses to visual stimuli, however this was also the case for our saline controls. All antipsychotic drugs tended to increase the fraction of neurons that, based on their correlation with visual flow (negative) and running (positive), are consistent with computing a mismatch response. This trend was opposed to saline and a pro-psychotic agent, and, for clozapine, this trend was not present in layer 5. Neural activity correlation with visual flow was changed more uniformly with antipsychotic medication, whereas correlation of neural activity with running was changed diversely, possibly indicating a more specific targeting of neuronal subpopulations responsive to motor prediction-related signals. It is conceivable, that with more data, one could confirm that these trends reflect a common functional signature.

We investigated mechanisms that explain the observed mismatch amplitude decrease post Clozapine. We found that SST neurons decrease their amplitude during mismatch, thereby contributing to the reduction in response (i.e. reducing the disinhibitory activity during mismatch events). We find that SST neurons likely change their correlation with running post Clozapine to become less running correlated, yet more visually correlated, having a reduced mean activity. We find that not only

mismatch response amplitudes are decreased, but visual response amplitudes as well, indicating a reduction in overall gain, besides the reduction in mean activity. These results point towards SSTs as potential mediators of antipsychotics triggering a reduction in prediction error responses in V1. However, it is unclear if this relationship is causal. One could increase the excitability of SSTs post clozapine treatment and to possibly observe a restoration of the mismatch response.

A study (Michaiel et al., 2019) quantified effects of hallucinogens on visual signals during stationary and moving periods found an overall reduction in visual signals. Another compound used to model psychosis pharmacologically was an NMDA receptor antagonist (MK801), and it also lowered visual responses. Three possibilities explain these findings: a) less feed-forward excitation or b) more top-down suppression, and/or c) local and direct suppression of activity. By inactivating anterior cingulate cortex (ACC) with muscimol, Ranson and colleagues (Ranson et al., 2019) show that input from ACC acts to inhibit V1 under the influence of MK801, and suggest an increase in top-down suppression as an explanation for this finding. We know that ACC likely sends predictive signals of visual flow to V1 (Leinweber et al., 2017) and given that there is a substantial amount of activity in V1 in absence of visual input (Keller et al., 2012), it is conceivable that predictive activity input to V1 is altered in psychosis, consistent with an imprecise internal model.

We find antipsychotic agents did not directly act to oppose a local suppression of visual responses, as visual signals (response to stimuli and activity correlation with visual flow) did not increase compared to saline controls (and may even further decrease). In fact, we found that motor-related responses seem to be either increased (Clozapine, Aripiprazole) or unchanged, and correlation with visual flow is significantly decreased post Haloperidol. Previous research speculated that the reduction of responses to visual stimuli may reflect an overweighing of signals reflecting expectations (Michaiel et al., 2019). If antipsychotics agents and pro-psychotic agents in V1 of healthy mice indeed have opposing effects, our findings suggest a more elaborate explanation.

It is unclear how antipsychotics influence visuomotor prediction error responses. Interestingly, we found an increase in running onset response and running correlation post CLO and ARI, yet a decrease in mismatch response. Given that the mismatch response scales with running speed (Zmarz and Keller, 2016), and assuming running responses are proxy for predictive weight, this is a remarkable difference. This could be explained by a) a structural change of signals onto mismatch neurons or b) an increase in motor-related responses not predictive of visual flow (less specificity) or both. Further analysis and experiments may reveal if the scaling of visuomotor mismatch and running is significantly different post CLO and post saline; unfortunately, we do not have enough data to answer this conclusively.

The trend that more neurons show correlations consistent with mismatch computation post antipsychotic drug, yet tend to be less responsive (ARI, CLO), might indicate a structural change, where more neurons are recruited for mismatch computation. Indeed, some in-vitro evidence exists, that dendritic spines of cortical neurons (in rats) are systematically changed by antipsychotic agents (Takaki et al., 2018) within days; cultured neurons showed more spines post Clozapine and Aripiprazole, yet less post Haloperidol compared to controls. This difference may also help to explain why Haloperidol does not affect mismatch in this study. Multiple structural changes that take some time to manifest may be one of the reasons why therapeutic benefits are not usually apparent immediately after drug administration in patients. Psychosis has been suggested to result from an inaccurately internal model given the available to the sensory data (Sterzer et al., 2018), thereby giving rise to faulty predictions (and prediction errors). By changing the input specificity of (predictive signals onto) mismatch neurons, faulty prediction errors may integrate predictions of other types, carry less weight in terms of updating the internal model and therefore lead to a gradual improvement of the internal model. Alternatively, visual signals and motor-related signals may be a poor proxy for the input onto mismatch neurons.

This study has limitations. We assume, that antipsychotics in healthy mice show trends that would correct a malfunctioning circuit configuration. It is, however, unclear if antipsychotic medication in healthy humans (or rodents) leads to changes that reflect beneficial effects seen in patients suffering from psychiatric disease. If further studies using mouse models of psychiatric diseases (e.g., DISC1 mice) find similar changes and trends as presented here, this could reduce (but not remove) this limitation. To address this limitation, more compounds could be tested and compared. Although, this study does not definitively define a clear functional signature for screening anti-psychotics in V1, it does suggest that examining how a compound affects sensorimotor mismatch response in primary visual cortex may be a reasonable approach classify newer antipsychotics and might help identify novel compounds of interest, and possibly predict clinical outcome better than previous animal models that have been plagued by previous limitations (Jones et al., 2011).

This study highlights the importance of studying antipsychotic action in cortical areas, and further research with larger sample sizes may show whether trends in the data hold up to more rigorous scrutiny. Systematically characterizing more antipsychotic medications and contrasting it with different pro-psychotic drugs on a larger scale may highlight more important differences, that could help to understand perceptual changes associated in psychiatric diseases.

SUPPLEMENTARY FIGURES

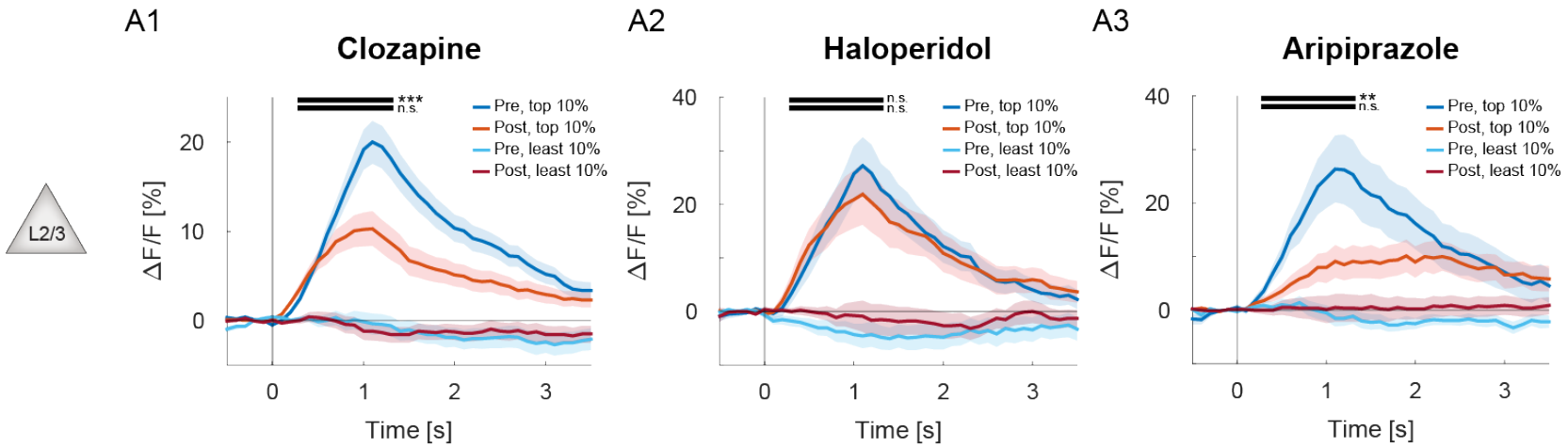

Figure S1. Related to Figure 1. Mismatch decreases due to neurons responding with increased firing rate.

(**A**) **A1**: 10% highest (blue, red) and lowest (light blue, dark red) responding neurons to mismatch onset, pre (blue) and post (red) Clozapine injection. **A2-3**: same as **A1** but post Haloperidol and Aripiprazole.

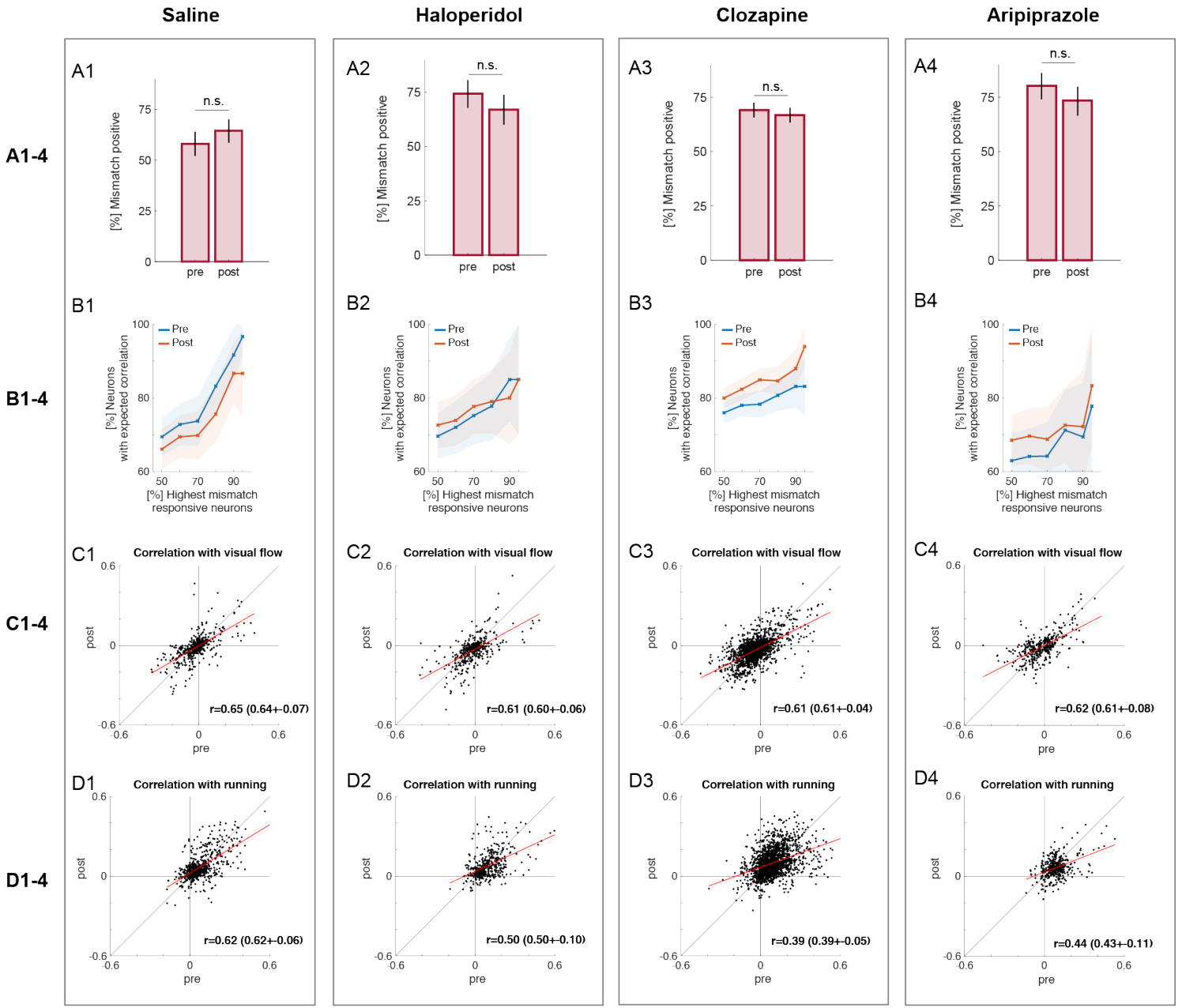
Saline
Haloperidol
Clozapine
Aripiprazole
A1-4
B1-4
C1-4
D1-4
A1
A2
A3
A4
n.s.
[%] Mismatch positive
pre
post
B1
B2
B3
B4
Pre
Post
[%] Neurons with expected correlation
[%] Highest mismatch responsive neurons
C1
C2
C3
C4
Correlation with visual flow
r=0.65 (0.64+-0.07)
r=0.61 (0.60+-0.06)
r=0.61 (0.61+-0.04)
r=0.62 (0.61+-0.08)
D1
D2
D3
D4
Correlation with running
r=0.62 (0.62+-0.06)
r=0.50 (0.50+-0.10)
r=0.39 (0.39+-0.05)
r=0.44 (0.43+-0.11)

Figure S2. Related to Figure 2.

(**A**) Fraction of neurons [%] with increased firing rate to mismatch onset pre (left) and post (right) drug injection. Error bars indicate 95% confidence interval from bootstrap (10'000 repeats, with replacement). n.s.: confidence interval overlaps.

(**B**) **B1**: Fraction of neurons [%] with positive activity correlation to running and negative to visual flow of all neurons (Y-axis) that showed an increased calcium response to mismatch onsets on average, as a function of increasing percentile cut-offs of highest-responding cells to mismatch (X-axis) pre (blue) and post (red) saline. **B2-4**: same as **B1** for HAL, CLO, ARI. Shading indicates 95% confidence interval of from bootstrap (10'000 repeats, with replacement). No significance testing has been performed.

(**C**) **C1**: Correlation of activity of every neuron with visual flow pre (X-axis) and post (Y-axis) saline injection. **C2-4**: same as **C1** for Hal, CLO, ARI. Red line indicates a linear fit to the data (see Methods).

(**D**) Same as (**C**) but for correlation with running.

1437

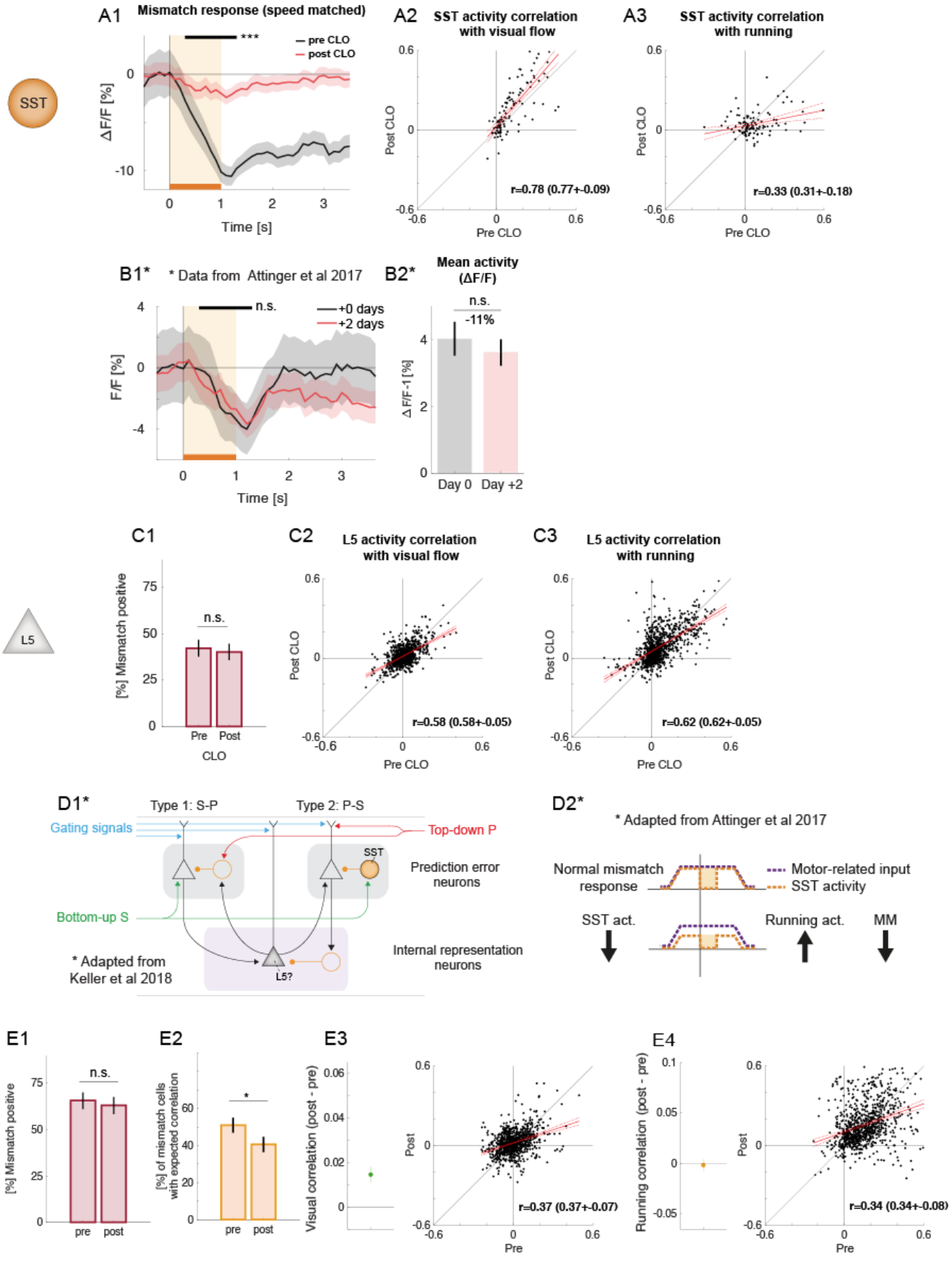
A1
Mismatch response (speed matched)
***
pre CLO
post CLO
ΔF/F [%]
Time [s]
A2
SST activity correlation with visual flow
Post CLO
Pre CLO
r=0.78 (0.77+-0.09)
A3
SST activity correlation with running
r=0.33 (0.31+-0.18)
SST
B1*
* Data from Attinger et al 2017
n.s.
+0 days
+2 days
F/F [%]
Time [s]
B2*
Mean activity (ΔF/F)
n.s.
-11%
Δ F/F -1 [%]
Day 0
Day +2
L5
C1
[%] Mismatch positive
n.s.
Pre
Post
CLO
C2
L5 activity correlation with visual flow
r=0.58 (0.58+-0.05)
C3
L5 activity correlation with running
r=0.62 (0.62+-0.05)
D1*
Type 1: S-P
Type 2: P-S
Gating signals
Top-down P
SST
Prediction error neurons
Bottom-up S
Internal representation neurons
L5?
* Adapted from Keller et al 2018
D2*
* Adapted from Attinger et al 2017
Normal mismatch response
Motor-related input
SST activity
SST act.
Running act.
MM
E1
[%] Mismatch positive
n.s.
pre
post
E2
[%] of mismatch cells with expected correlation
*
E3
Visual correlation (post - pre)
Post
Pre
r=0.37 (0.37+-0.07)
E4
Running correlation (post - pre)
r=0.34 (0.34+-0.08)

Figure S3. Related to Figure 3.

(**A**) **A1**: Speed-matched (see Methods) SST response to mismatch from (Attinger et al., 2017) at day 1 (black) and two days later (red). Shading indicates SEM over neurons. No rejection of null hypothesis by rank-sum over mean responses by neuron indicated time interval (horizontal black line, top).

A2: Correlation of activity of every neuron with visual flow pre (X-axis) and post (Y-axis) Clozapine injection. Red line indicates a linear fit to the data (see Methods).

A3: Same as **A2**, but for correlation with running.

(**B**) Fraction of layer 5 neurons [%] with increased firing rate to mismatch onset. Error bars indicate 95% confidence interval from bootstrap (10'000 repeats, with replacement). n.s.: confidence interval overlaps.

(**B**) **B1**: Mismatch response (ΔF/F [%]) at first imaging timepoint (day 0) and later (day +2), averaged over trials and SST neurons; error bar shading indicates SEM over neurons. Orange shading and horizontal bar indicate onset and duration of visual flow halt. Significance was tested using rank-sum for the black, horizontal bar (top). Legend: * $p<0.05$, ** $p<0.01$, *** $p<0.001$.

B2: Mean activity (ΔF/F [%] - 1) for Day 0 and Day +2 during the whole experiment. Error bars indicate SEM over neurons. Activity was not different for those two timepoints (p=, rank-sum test).

(**C**) **C1**: Fraction of layer 5 neurons [%] with increased firing rate to mismatch onset. Error bars indicate 95% confidence interval from bootstrap (10'000 repeats, with replacement). n.s.: confidence interval overlaps.

C2: Correlation of activity of every layer 5 neuron with visual flow pre (X-axis) and post (Y-axis) Clozapine injection. Red line indicates a linear fit to the data (see Methods).

C3: same as **C2**, but for running correlation.

(D) D1: Decreased mean activity in SST neurons reduce mismatch response (chemogenic inactivation). Adapted from (Attinger et al., 2017).

D2 Predictive processing schematic from (Keller and Mrsic-Flogel, 2018).

(**E**) Changes post pro-psychotic drug injection (see Methods). **E1**: Fraction of neurons [%] with increased firing rate to mismatch onset. Error bars indicate 95% confidence interval from bootstrap (10'000 repeats, with replacement). n.s.: confidence interval overlaps.

E2: Fraction of neurons [%] with positive activity correlation to running and negative to visual flow of all neurons that showed an increased calcium response to mismatch onsets on average. Numbers on top of the bars indicate the absolute number of neurons with positive mismatch response. Error bars indicate 95% confidence interval obtained by bootstrap (10'000 repeats, with replacement). * indicates confidence intervals do not overlap (n.s. indicates they overlap).

E3: Left: Quantification of mean shift (post-pre) of every neuron's average visual correlation. Right: Correlation of activity of every neuron with visual flow pre (X-axis) and post (Y-axis) pro-psychotic agent. Red line indicates a linear fit to the data (see Methods).

E4: Same as **E3** but for correlation with running.

METHODS

Animals and surgery

All animal procedures that led to the results of this paper were approved by and carried out in accordance with Swiss guidelines of Canton Basel Stadt's Veterinary Department guidelines. For two-photon and behavioral experiments, mice were anesthetized with a standardized solution of Fentanyl (0.05 mg/kg; Actavis), Midazolam (5.0 mg/kg; Dormicum, Roche) and Medetomidine (0.5 mg/kg; Domitor, Orion). Eyes were carefully covered with ophthalmic gel (Virbac Schweiz AG). Analgesics were applied perioperatively (2% Lidocaine gel, Bichsel AG, Meloxicam 5mg/kg; Metacam, Boehringer Ingelheim) and post-operatively (Buprenorphine 0.1g/kg, Reckitt Benckiser Healthcare Ltd.). We performed a standardized cranial window surgery of 4mm diameter (described in detail here: (Leinweber et al., 2014; Zmarz and Keller, 2016)) bilaterally, following injections of ca. 200nl of AAV virus (AAV2/1-EF1α-GCaMP6f-WPRE) into the target area primary visual cortex (V1, right hemisphere), centered 2.5±.3mm AP/ML from lambda.

Imaging and animal summary

All mice used had the same genetic background (C57BL/6) and were between the age of 76 – 135 days postpartum and of the following strain:

C57BL/6J	from Charles River
SST-Cre	from Jackson Laboratory (Nr. 018973)

All animals received approximately 4-8h of visuomotor exposure (closed-loop) prior to first imaging timepoint to get the animals accustomed to the virtual reality setup and increase average running speed. The saline group included 7, Haloperidol 10, Clozapine 16 and Aripiprazole 8 mice. Imaging was performed as described in the previous chapter of this thesis.

Drug information, preparation, and choice of dosage

Clozapine (SA; 0.1mg/kg), Aripiprazole (Otsuka Pharmaceutical GmbH; 0.1mg/kg), Haloperidol (Janssen-Cilag AG; 0.1mg/kg), pro-psychotic agent A (gifted; 150µg/kg), (+)-MK-801 hydrogen maleate (SA; 0.1mg/kg), Ketamine (local pharmacy, 50mg/kg). All drugs were injected intraperitoneally.

Aripiprazole and Haloperidol were diluted in 0.9% NaCl solution of 10ml. Clozapine was dissolved with HCl, then diluted with 0.9% NaCl. All solutions were mixed to a 'stock solution' of 10ml and a concentration of 1mg/ml and stored in a fridge for less than three months. Stock solutions were then further diluted to 'working solutions', at a concentration of 10µg/ml, which then was injected

intraperitoneally. For Clozapine, we checked that the pH of the working solution is approximately the same as 0.9% NaCl solution.

Because we know running behavior affects responses we measure during these experiments, we aimed to find the maximum dose that did not systematically decrease the running behavior of the animals. We ran a small pilot study exploring different dosages and locomotive effects and measured the change in running behavior, which determined the dosage we used (data not shown).

Viral constructs and mouse strains

AAV2/1-EF1α-GCaMP6f-WPRE	from FMI vector core
AAV2/1-EF1α-DIO-GCaMP6f-WPRE	from FMI vector core

Data, code, and resource sharing

Information about vectors from FMI vector core: vector.fmi.ch. Data and code to generate all figures of this chapter, and resource sharing: Please contact the lab head, Georg Keller.

Data analysis

All data analysis was performed with custom analysis scripts in MATLAB 2020b. For all population onset responses, data was averaged over onsets and concatenated over neurons. Unless otherwise stated, the shading of the error bars indicates the standard error of the mean (SEM) over the average neuron response. Unless otherwise stated in figure legends, horizontal bars above neuronal population responses denoted the window of significance test (+300 to +1300ms), same as in **Chapter I**. MM+ neurons were defined as neurons with an average response greater than zero in the significance window post mismatch onset. Speed matching was achieved by sequentially removing the 99^{th} and 1^{st} percentile of all trials concatenated for an onset of interest. This was repeated until a stop condition was met: 1) the Kolmogorov-Smirnov distance of running speeds in a window (-500ms to +500ms) was not significantly different ($p>0.05$), 2) average difference between all onsets in the window was low (less than 0.005). 3) less than 33% of trials remain (unsuccessful match). For linear fit models, the standard implementation in MATLAB was used. The solid (red) line denotes the simple linear fit using one predictor variable, the dotted lines denote 95% confidence intervals.

CONCLUSIONS AND EPILOGUE

In **Chapter I**, we found that development of visuomotor mismatch responses is impaired if NMDA receptors are knocked out, or CaMKII inhibited, during early development of visual cortex. This impairment also affected visuomotor skill learning later in life. In **Chapter II**, we characterized changes in primary visual cortex in response to antipsychotic agents and found evidence that visuomotor prediction error responses are decreased for the atypical antipsychotic agents that we tested.

Psychiatric diseases have a developmental component, and one of the prevailing hypotheses is a global NMDA receptor hypofunction. Our results are consistent with the hypothesis that NMDA receptor hypofunction during developmental phases development leads to altered prediction error responses, that may cause behavioral deficits. Functional end-point of antipsychotic agents may be a change in top-down signals, that reflects a change of prediction specificity or weight, resulting in changes of prediction errors and a change in how the internal model is updated. Further research may address this by quantifying the change of antipsychotics on the top-down input to V1.

REFERENCES

Attinger, A., Wang, B., and Keller, G.B. (2017). Visuomotor Coupling Shapes the Functional Development of Mouse Visual Cortex. Cell *169*, 1291-1302.e14.

Barria, A., and Malinow, R. (2005). NMDA receptor subunit composition controls synaptic plasticity by regulating binding to CaMKII. Neuron *48*, 289–301.

Bickford, M.E., Slusarczyk, A., Dilger, E.K., Krahe, T.E., Kucuk, C., and Guido, W. (2010). Synaptic development of the mouse dorsal lateral geniculate nucleus. J. Comp. Neurol. *518*, 622–635.

Bouvier, G., Larsen, R.S., Rodríguez-Moreno, A., Paulsen, O., and Sjöström, P.J. (2018). Towards resolving the presynaptic NMDA receptor debate. Curr. Opin. Neurobiol. *51*, 1–7.

Bramness, J.G., Gundersen, Ø.H., Guterstam, J., Rognli, E.B., Konstenius, M., Løberg, E.M., Medhus, S., Tanum, L., and Franck, J. (2012). Amphetamine-induced psychosis - a separate diagnostic entity or primary psychosis triggered in the vulnerable? BMC Psychiatry *12*, 221.

Brown, T.B., Mann, B., Ryder, N., Subbiah, M., Kaplan, J., Dhariwal, P., Neelakantan, A., Shyam, P., Sastry, G., Askell, A., et al. (2020). Language Models are Few-Shot Learners. ArXiv.

Callaway, E.M. (2002). Cell type specificity of local cortical connections. J. Neurocytol. *31*, 231–237.

Carpenter, W.T., and Davis, J.M. (2012). Another view of the history of antipsychotic drug discovery and development. Mol. Psychiatry *17*, 1168–1173.

Chiu, C.Q., Martenson, J.S., Yamazaki, M., Natsume, R., Sakimura, K., Tomita, S., Tavalin, S.J., and Higley, M.J. (2018). Input-Specific NMDAR-Dependent Potentiation of Dendritic GABAergic Inhibition. Neuron *97*, 368-377.e3.

Clark, A. (2013). Whatever next? Predictive brains, situated agents, and the future of cognitive science. Behav. Brain Sci. *36*, 181–204.

Clark, A. (2016). Surfing uncertainty : prediction, action, and the embodied mind (Oxford University Press).

Cruz-Martín, A., El-Danaf, R.N., Osakada, F., Sriram, B., Dhande, O.S., Nguyen, P.L., Callaway, E.M., Ghosh, A., and Huberman, A.D. (2014). A dedicated circuit links direction-selective retinal ganglion cells to the primary visual cortex. Nature *507*, 358–361.

D'Souza, R.S., and Hooten, W.M. (2021). Extrapyramidal Symptoms. (Treasure Island (FL)), p.

Dombeck, D.A., Khabbaz, A.N., Collman, F., Adelman, T.L., and Tank, D.W. (2007). Imaging large-scale neural activity with cellular resolution in awake, mobile mice. Neuron *56*, 43–57.

Erisken, S., Vaiceliunaite, A., Jurjut, O., Fiorini, M., Katzner, S., and Busse, L. (2014). Effects of

locomotion extend throughout the mouse early visual system. Curr. Biol. *24*, 2899–2907.

Farooq, S., Choudry, A., Cohen, D., Naeem, F., and Ayub, M. (2019). Barriers to using clozapine in treatment-resistant schizophrenia: systematic review. BJPsych Bull. *43*, 8–16.

Farrer, C., Franck, N., Georgieff, N., Frith, C.D., Decety, J., and Jeannerod, M. (2003). Modulating the experience of agency: A positron emission tomography study. Neuroimage *18*, 324–333.

Fletcher, P.C., and Frith, C.D. (2009). Perceiving is believing: a Bayesian approach to explaining the positive symptoms of schizophrenia. Nat. Rev. Neurosci. *10*, 48–58.

Fong, M.F., Finnie, P.S., Kim, T., Thomazeau, A., Kaplan, E.S., Cooke, S.F., and Bear, M.F. (2020). Distinct Laminar Requirements for NMDA Receptors in Experience-Dependent Visual Cortical Plasticity. Cereb. Cortex *30*, 2555–2572.

Forrest, D., Yuzaki, M., Soares, H.D., Ng, L., Luk, D.C., Sheng, M., Stewart, C.L., Morgan, J.I., Connor, J.A., and Curran, T. (1994). Targeted disruption of NMDA receptor 1 gene abolishes NMDA response and results in neonatal death. Neuron *13*, 325–338.

Franklin, D.W., and Wolpert, D.M. (2011). Computational mechanisms of sensorimotor control. Neuron *72*, 425–442.

Franklin, K.B.J., and Paxinos, G. (2012). Paxinos and Franklin's The mouse brain in stereotaxic coordinates, 4th Edition. (Elsevier).

Friston, K. (2005). A theory of cortical responses. Philos. Trans. R. Soc. Lond. B. Biol. Sci. *360*, 815–836.

Gambrill, A.C., and Barria, A. (2011). NMDA receptor subunit composition controls synaptogenesis and synapse stabilization. Proc. Natl. Acad. Sci. U. S. A. *108*, 5855–5860.

Grienberger, C., and Konnerth, A. (2012). Imaging Calcium in Neurons. Neuron *73*, 862–885.

Gu, X., Zhou, L., and Lu, W. (2016). An NMDA Receptor-Dependent Mechanism Underlies Inhibitory Synapse Development. Cell Rep. *14*, 471–478.

Guo, Z. V., Inagaki, H.K., Daie, K., Druckmann, S., Gerfen, C.R., and Svoboda, K. (2017). Maintenance of persistent activity in a frontal thalamocortical loop. Nature *545*, 181–186.

Halberstadt, A.L., Van Der Heijden, I., Ruderman, M.A., Risbrough, V.B., Gingrich, J.A., Geyer, M.A., and Powell, S.B. (2009). 5-HT 2A and 5-HT 2C receptors exert opposing effects on locomotor activity in mice. Neuropsychopharmacology *34*, 1958–1967.

Hamm, J.P., Peterka, D.S., Gogos, J.A., and Yuste, R. (2017). Altered Cortical Ensembles in Mouse Models of Schizophrenia. Neuron *94*, 153-167.e8.

Hartline, H.K. (1938). The response of single optic nerve fibers of the vertebrate eye to illumination of the retina. Am. J. Physiol. Content *121*, 400–415.

Hasan, M.T., Hernández-González, S., Dogbevia, G., Treviño, M., Bertocchi, I., Gruart, A., and Delgado-García, J.M. (2013). Role of motor cortex NMDA receptors in learning-dependent synaptic plasticity of behaving mice. Nat. Commun. *4*, 2258.

Hebb, D.O. (1949). The organization of behavior; a neuropsychological theory. (Oxford, England: Wiley).

Hein, A., and Held, R. (1967). Dissociation of the visual placing response into elicited and guided components. Science *158*, 390–392.

Heindorf, M., Arber, S., and Keller, G.B. (2018). Mouse Motor Cortex Coordinates the Behavioral Response to Unpredicted Sensory Feedback. Neuron *99*, 1040-1054.e5.

Held, R., and Hein, A. (1963). Movement-produced stimulation in the development of visually guided behavior. J. Comp. Physiol. Psychol. *56*, 872–876.

Herring, B.E., and Nicoll, R.A. (2016). Long-Term Potentiation: From CaMKII to AMPA Receptor Trafficking. Annu. Rev. Physiol. *78*, 351–365.

von Holst, E., and Mittelstaedt, H. (1950). Das Reafferenzprinzip. Naturwissenschaften *37*, 464–476.

Hooks, B.M., and Chen, C. (2020). Circuitry Underlying Experience-Dependent Plasticity in the Mouse Visual System. Neuron *106*, 21–36.

Hubel, D., and Wiesel, T. (1962). Receptive fields, binocular interaction and functional architecture in the cat's visual cortex. J. Physiol. *160*, 106.

Huberman, A.D., and Niell, C.M. (2011). What can mice tell us about how vision works? Trends Neurosci. *34*, 464–473.

Huhn, M., Nikolakopoulou, A., Schneider-Thoma, J., Krause, M., Samara, M., Peter, N., Arndt, T., Bäckers, L., Rothe, P., Cipriani, A., et al. (2019). Comparative efficacy and tolerability of 32 oral antipsychotics for the acute treatment of adults with multi-episode schizophrenia: a systematic review and network meta-analysis. Lancet *394*, 939–951.

Ibrahim, L.A., Mesik, L., Ji, X. ying, Fang, Q., Li, H. fu, Li, Y. tang, Zingg, B., Zhang, L.I., and Tao, H.W. (2016). Cross-Modality Sharpening of Visual Cortical Processing through Layer-1-Mediated Inhibition and Disinhibition. Neuron *89*, 1031–1045.

Jones, C., Watson, D., and Fone, K. (2011). Animal models of schizophrenia. Br. J. Pharmacol. *164*, 1162–1194.

Jordan, R., and Keller, G.B. (2020). Opposing Influence of Top-down and Bottom-up Input on Excitatory Layer 2/3 Neurons in Mouse Primary Visual Cortex. Neuron *108*, 1194-1206.e5.

Keller, G.B., and Hahnloser, R.H.R. (2009). Neural processing of auditory feedback during vocal practice in a songbird. Nature *457*, 187–190.

Keller, G.B., and Mrsic-Flogel, T.D. (2018). Predictive Processing: A Canonical Cortical Computation. Neuron *100*, 424–435.

Keller, A.J., Roth, M.M., and Scanziani, M. (2020). Feedback generates a second receptive field in neurons of the visual cortex. Nature *582*, 545–549.

Keller, G.B., Bonhoeffer, T., and Hübener, M. (2012). Sensorimotor Mismatch Signals in Primary Visual Cortex of the Behaving Mouse. Neuron *74*, 809–815.

Lein, E.S. et al. (2007). Allen Mouse Brain Atlas : Genome-wide atlas of gene expression in the adult mouse brain. Nature 168–176.

Leinweber, M., Zmarz, P., Buchmann, P., Argast, P., Hübener, M., Bonhoeffer, T., and Keller, G.B. (2014). Two-photon calcium imaging in mice navigating a virtual reality environment. J. Vis. Exp. e50885.

Leinweber, M., Ward, D.R., Sobczak, J.M., Attinger, A., and Keller, G.B. (2017). A Sensorimotor Circuit in Mouse Cortex for Visual Flow Predictions. Neuron *95*, 1420-1432.e5.

Leonard, A.S., Lim, I.A., Hemsworth, D.E., Horne, M.C., and Hell, J.W. (1999). Calcium/calmodulin-dependent protein kinase II is associated with the N-methyl-D-aspartate receptor. Proc. Natl. Acad. Sci. U. S. A. *96*, 3239–3244.

Leucht, S., Corves, C., Arbter, D., Engel, R.R., Li, C., and Davis, J.M. (2009). Second-generation versus first-generation antipsychotic drugs for schizophrenia: a meta-analysis. Lancet *373*, 31–41.

Leucht, S., Leucht, C., Huhn, M., Chaimani, A., Mavridis, D., Helfer, B., Samara, M., Rabaioli, M., Bächer, S., Cipriani, A., et al. (2017). Sixty years of placebo-controlled antipsychotic drug trials in acute schizophrenia: Systematic review, Bayesian meta-analysis, and meta-regression of efficacy predictors. Am. J. Psychiatry *174*, 927–942.

Lillicrap, T.P., Santoro, A., Marris, L., Akerman, C.J., and Hinton, G. (2020). Backpropagation and the brain. Nat. Rev. Neurosci. *21*, 335–346.

Lisman, J., Yasuda, R., and Raghavachari, S. (2012). Mechanisms of CaMKII action in long-term potentiation. Nat. Rev. Neurosci. *13*, 169–182.

Lo, F.S., Akkentli, F., Tsytsarev, V., and Erzurumlu, R.S. (2013). Functional significance of cortical NMDA receptors in somatosensory information processing. J. Neurophysiol. *110*, 2627–2636.

López-Muñoz, F., Alamo, C., Cuenca, E., Shen, W.W., Clervoy, P., and Rubio, G. (2005). History of the discovery and clinical introduction of chlorpromazine. Ann. Clin. Psychiatry *17*, 113–135.

Magee, J.C., and Grienberger, C. (2020). Synaptic Plasticity Forms and Functions. Annu. Rev. Neurosci. *43*, 95–117.

Marr, D. (1982). Vision (MIT Press).

Martin, S.J., Grimwood, P.D., and Morris, R.G.M. (2000). Synaptic plasticity and memory: An evaluation of the hypothesis. Annu. Rev. Neurosci. *23*, 649–711.

Masland, R.H., and Martin, P.R. (2007). The unsolved mystery of vision. Curr. Biol. *17*.

Michaiel, A.M., Parker, P.R.L., and Niell, C.M. (2019). A Hallucinogenic Serotonin-2A Receptor Agonist Reduces Visual Response Gain and Alters Temporal Dynamics in Mouse V1. Cell Rep. *26*, 3475-3483.e4.

Mitra, N.J., Chu, H.K., Lee, T.Y., Wolf, L., Yeshurun, H., and Cohen-Or, D. (2009). Emerging Images. ACM Trans. Graph. *28*, 1–8.

Monyer, H., Burnashev, N., Laurie, D.J., Sakmann, B., and Seeburg, P.H. (1994). Developmental and regional expression in the rat brain and functional properties of four NMDA receptors. Neuron *12*, 529–540.

Morin, L.P., and Studholme, K.M. (2014). Retinofugal projections in the mouse. J. Comp. Neurol. *522*, 3733–3753.

Murakoshi, H., Shin, M.E., Parra-Bueno, P., Szatmari, E.M., Shibata, A.C.E., and Yasuda, R. (2017). Kinetics of Endogenous CaMKII Required for Synaptic Plasticity Revealed by Optogenetic Kinase Inhibitor. Neuron *94*, 37-47.e5.

Nicholls, M.E.R., Churches, O., and Loetscher, T. (2018). Perception of an ambiguous figure is affected by own-age social biases. Sci. Rep. *8*, 12661.

Niell, C.M., and Stryker, M.P. (2010). Modulation of visual responses by behavioral state in mouse visual cortex. Neuron *65*, 472–479.

Nucifora, F.C., Mihaljevic, M., Lee, B.J., and Sawa, A. (2017). Clozapine as a Model for Antipsychotic Development. Neurotherapeutics *14*, 750–761.

Olshausen, B.A., and Field, D.J. (2009). What Is the Other 85 Percent of V1 Doing? In 23 Problems in Systems Neuroscience, (Oxford University Press), p.

Paoletti, P., Bellone, C., and Zhou, Q. (2013). NMDA receptor subunit diversity: Impact on receptor properties, synaptic plasticity and disease. Nat. Rev. Neurosci. *14*, 383–400.

Petreanu, L., Mao, T., Sternson, S.M., and Svoboda, K. (2009). The subcellular organization of neocortical excitatory connections. Nature *457*, 1142–1145.

Plato “The Allegory of the Cave” excerpt from The Republic (360 BC). Translation retrieved from https://human.libretexts.org/@go/page/40388 05-Apr-2021.

Ramachandraiah, C.T., Subramaniam, N., and Tancer, M. (2009). The story of antipsychotics: Past and present. Indian J. Psychiatry *51*, 324–326.

Ranson, A., Broom, E., Powell, A., Chen, F., Major, G., and Hall, J. (2019). Top-Down Suppression of Sensory Cortex in an NMDAR Hypofunction Model of Psychosis. Schizophr. Bull. *45*, 1349–1357.

Rao, R.P., and Ballard, D.H. (1999). Predictive coding in the visual cortex: a functional

interpretation of some extra-classical receptive-field effects. Nat. Neurosci. *2*, 79–87.

Reichert, D.P., Seriès, P., and Storkey, A.J. (2013). Charles Bonnet Syndrome: Evidence for a Generative Model in the Cortex? PLoS Comput. Biol. *9*, 1003134.

Roelfsema, P.R., and Holtmaat, A. (2018). Control of synaptic plasticity in deep cortical networks. Nat. Rev. Neurosci. *19*, 166–180.

Roman Originals The Dress: Roman Originals co-founder Peter Christodoulou on how viral image left company sitting pretty | The Independent (Katie Grant).

Rompani, S.B., Müllner, F.E., Wanner, A., Zhang, C., Roth, C.N., Yonehara, K., and Roska, B. (2017). Different Modes of Visual Integration in the Lateral Geniculate Nucleus Revealed by Single-Cell-Initiated Transsynaptic Tracing. Neuron *93*, 767-776.e6.

Sabatini, B.L., Oertner, T.G., and Svoboda, K. (2002). The life cycle of Ca2+ ions in dendritic spines. Neuron *33*, 439–452.

Saleem, A.B., Ayaz, A., Jeffery, K.J., Harris, K.D., and Carandini, M. (2013). Integration of visual motion and locomotion in mouse visual cortex. Nat. Neurosci. *16*, 1864–1869.

Sawtell, N.B., Frenkel, M.Y., Philpot, B.D., Nakazawa, K., Tonegawa, S., and Bear, M.F. (2003). NMDA receptor-dependent ocular dominance plasticity in adult visual cortex. Neuron *38*, 977–985.

Schnabel, U.H., Kirchberger, L., van Beest, E.H., Mukherjee, S., Barsegyan, A., Lorteije, J.A.M., van der Togt, C., Self, M.W., and Roelfsema, P.R. (2018). Feedforward and feedback processing during figure-ground perception in mice. BioRxiv 456459.

Seabrook, T.A., Burbridge, T.J., Crair, M.C., and Huberman, A.D. (2017). Architecture, Function, and Assembly of the Mouse Visual System. Annu. Rev. Neurosci. *40*, 499–538.

Sherrington, C.S. (1906). Observations on the scratch-reflex in the spinal dog. J. Physiol. *34*, 1–50.

Simons, D.J., and Chabris, C.F. (1999). Gorillas in our midst: Sustained inattentional blindness for dynamic events. Perception *28*, 1059–1074.

Spratling, M.W. (2017). A review of predictive coding algorithms. Brain Cogn. *112*, 92–97.

Stanley, J., and Miall, R.C. (2007). Functional activation in parieto-premotor and visual areas dependent on congruency between hand movement and visual stimuli during motor-visual priming. Neuroimage *34*, 290–299.

Sterzer, P., Adams, R.A., Fletcher, P., Frith, C., Lawrie, S.M., Muckli, L., Petrovic, P., Uhlhaas, P., Voss, M., and Corlett, P.R. (2018). The Predictive Coding Account of Psychosis. Biol. Psychiatry *84*, 634–643.

Takaki, M., Kodama, M., Mizuki, Y., Kawai, H., Yoshimura, B., Kishimoto, M., Sakamoto, S., Okahisa, Y., and Yamada, N. (2018). Effects of the antipsychotics haloperidol, clozapine, and aripiprazole on the dendritic spine. Eur.

Neuropsychopharmacol. *28*, 610–619.

Tsien, J.Z., Chen, D.F., Gerber, D., Tom, C., Mercer, E.H., Anderson, D.J., Mayford, M., Kandel, E.R., and Tonegawa, S. (1996). Subregion- and cell type-restricted gene knockout in mouse brain. Cell *87*, 1317–1326.

Tungaraza, T.E., and Farooq, S. (2015). Clozapine prescribing in the UK: Views and experience of consultant psychiatrists. Ther. Adv. Psychopharmacol. *5*, 88–96.

Vollenweider, F.X., Vollenweider-Scherpenhuyzen, M.F.I., Bäbler, A., Vogel, H., and Hell, D. (1998). Psilocybin induces schizophrenia-like psychosis in humans via a serotonin-2 agonist action. Neuroreport *9*, 3897–3902.

de Vries, S.E.J., Lecoq, J.A., Buice, M.A., Groblewski, P.A., Ocker, G.K., Oliver, M., Feng, D., Cain, N., Ledochowitsch, P., Millman, D., et al. (2020). A large-scale standardized physiological survey reveals functional organization of the mouse visual cortex. Nat. Neurosci. *23*, 138–151.

Wade, K.A., Garry, M., Read, J.D., and Lindsay, D.S. (2002). A picture is worth a thousand lies: Using false photographs to create false childhood memories. Psychon. Bull. Rev. *9*, 597–603.

Wang, C.C., Held, R.G., Chang, S.C., Yang, L., Delpire, E., Ghosh, A., and Hall, B.J. (2011). A critical role for gluN2B-containing NMDA receptors in cortical development and function. Neuron *72*, 789–805.

Yona, G., Meitav, N., Kahn, I., and Shoham, S. (2016). Realistic numerical and analytical modeling of light scattering in brain tissue for optogenetic applications. ENeuro *3*, 420–424.

Young, H., Belbut, B., Baeta, M., and Petreanu, L. (2021). Laminar-specific cortico-cortical loops in mouse visual cortex. Elife *10*, 1–25.

Zmarz, P., and Keller, G.B. (2016). Mismatch Receptive Fields in Mouse Visual Cortex. Neuron *92*, 766–772.

1547

Curriculum vitae

Felix Widmer, felix.widmer@fmi.ch

Education

<2008	Basic school education Major: music, high school thesis: artificial neural networks.
2009	Language Exchange, TESOL English teaching certificate
2010-2016	Human medicine studies at university of Basel
2017-2021	MD PhD in Neuroscience, at Friedrich Miescher Institute (FMI), Basel Medical doctorate at University Hospital of Basel (Dr. med.)
≥2021	Resident in neurology at the university hospital Basel

Publications

2018 (MD thesis)	Overall bioburden by total colony count does not predict the presence of pathogens with high clinical relevance in hospital and community environments DOI: 10.1016/j.jhin.2018.11.014
2021 (PhD thesis)	NMDA receptors in visual cortex are necessary for normal visuomotor integration and skill learning DOI: 10.7554/eLife.71476